INVITED PAPER

Randomly-Coupled Multi-Core Fiber Technology

This article considers an even higher density spatially parallel integration technique that allows for random coupling between the cores of multi-core fibers.

By Tetsuya Hayashi, *Senior Member IEEE*, Taiji Sakamoto, *Member IEEE*, Yusuke Yamada, Roland Ryf, *Fellow IEEE*, René-Jean Essiambre, *Fellow IEEE*, Nicolas Fontaine, *Senior Member IEEE*, Mikael Mazur, *Member IEEE*, Haoshuo Chen, *Senior Member IEEE*, and Takemi Hasegawa, *Member IEEE*

ABSTRACT | Randomly-coupled multi-core fiber (MCF) technology has come to attract lots of attention because of its strong applicability to long-haul transmission systems. Compared with weakly-coupled MCFs with independent cores, it can simultaneously realize higher spatial channel density and ultralow transmission loss using existing ultralow-loss single-mode fiber (SMF) core designs. The strong mode coupling characteristics of randomly-coupled MCFs can provide favorable optical properties, such as suppressed accumulation of modal dispersion (MD), mode-dependent loss (MDL), and nonlinear impairments. This article gives an overview of randomly-coupled MCF technology advancements. First, we describe the classification and design of randomly-coupled MCFs and explain what the randomly-coupled MCFs are and how they are designed. State-of-the-art randomly-coupled MCFs can accommodate four, seven, or 12 cores in a standard 125-μm cladding while achieving ultralow transmission loss and/or small MD, which are very promising for long-haul transmission media. Next, we present the methods to characterize the optical properties of randomly-coupled MCFs and the difference compared to conventional SMF measurements. We also show the low-loss low-MDL connectivity of this type of MCF and the cabling that can suppress MD. A field-deployed randomly-coupled MCF cable testbed is also presented, which confirmed the favorable optical properties of randomly-coupled MCFs after deployment. Then, multi-core amplifier technologies are briefly summarized, and finally, we discuss the performance improvements in the transmissions over randomly-coupled MCFs and suitable application areas.

KEYWORDS | Erbium-doped fiber amplifiers (EDFAs); optical fiber communication; optical fibers; space-division multiplexing (SDM).

I. INTRODUCTION

Network traffic has been growing exponentially over the decades due to repeatedly emerging digital applications and services (such as cloud services, video streaming, and, most recently, the Internet of Things), and the transmission capacity through single-mode fibers (SMFs) has also exponentially increased to tackle ever-growing traffic demands thanks to various technological innovations, such as wavelength division multiplexing and higher order modulation with digital coherent technology [1]–[3]. However, SMF capacity is now approaching its fundamental limit in the efficiently amplifiable wavelength band [1], [4], [5]. To tackle this limitation, space-division multiplexing (SDM) technology has been intensively researched, and various multi-core fibers (MCFs) and few-mode fibers (FMFs) have been proposed for SDM transmission [6]–[9]. Today, SDM is recognized as the only practical way to multiply the transmission capacity of optical fibers [1]–[3], [10].

Among the various SDM fibers, randomly-coupled MCFs are one of the most promising transmission media for long-haul transmission, which is intentionally designed

Manuscript received 16 October 2021; revised 30 March 2022; accepted 2 June 2022. Date of publication 22 June 2022; date of current version 11 November 2022. *(Corresponding author: Tetsuya Hayashi.)*

Tetsuya Hayashi and **Takemi Hasegawa** are with the Optical Communications Laboratory, Sumitomo Electric Industries Ltd., Yokohama 244-8588, Japan (e-mail: t-hayashi@sei.co.jp; hase@sei.co.jp).

Taiji Sakamoto and **Yusuke Yamada** are with the NTT Access Networks Service Systems Laboratories, NTT Corporation, Tsukuba 305-0805, Japan (e-mail: taiji.sakamoto.un@hco.ntt.co.jp; yuusuke.yamada.ze@hco.ntt.co.jp).

Roland Ryf, **René-Jean Essiambre**, **Nicolas Fontaine**, **Mikael Mazur**, and **Haoshuo Chen** are with Nokia Bell Labs, Murray Hill, NJ 07974 USA (e-mail: roland.ryf@nokia-bell-labs.com; rene.essiambre@nokia-bell-labs.com; nicolas.fontaine@nokia-bell-labs.com; mikael.mazur@nokia-bell-labs.com; haoshuo.chen@nokia-bell-labs.com).

Digital Object Identifier 10.1109/JPROC.2022.3182049

to have random mode coupling between the multiple cores. By permitting random mode coupling, randomly-coupled MCFs can simultaneously realize ultralow loss and high spatial channel density [11]–[13] compared to other SDM fibers. Random mode coupling is also beneficial for suppressing the accumulation of modal dispersion (MD) [14]–[20], mode-dependent loss (MDL) [20]–[25], and nonlinear impairments [24], [26], [27]. Although multiple-input–multiple-output (MIMO) digital signal processing (DSP) is necessary for undoing mode mixing among the cores, ultralong-haul transmission over $>$12 000 km using off-line processing [24], [28] and real-time 7200-km transmission using online processing on a field-programmable gate array (FPGA) have been demonstrated [29]. Wideband transmission experiments have also been performed in the C-band [30] and in C + L-band [31].

This article gives an overview of randomly-coupled MCF technology. First, in Section II, we briefly discuss the classification of MCFs to understand what randomly-coupled MCFs discussed in this article are and what is different from other types of MCFs. Section III discusses the MCF designs to assure random mode coupling and the effects of fiber bends and twists on group delay spread (GDS) and introduces representative examples of reported randomly-coupled MCFs. Section IV describes how to characterize randomly-coupled MCFs: what parameters should be evaluated in a mode-averaged or mode-resolved manner, and what method should be used in their measurement. Section V reviews connectivity technologies for splicing and termination of randomly-coupled MCFs, cabling technologies and fabrication results, and the world's first field deployment and characterization of an MCF cable. Section VI reviews MCF amplifier technologies applicable to randomly-coupled MCF amplification. Section VII describes transmission experiments over randomly-coupled MCFs, shows performance improvements in nonlinear transmissions, and also discusses suitable applications for randomly-coupled MCFs. Section VIII concludes this article.

II. MULTI-CORE FIBER CLASSIFICATION

MCFs can be divided into weakly-coupled MCFs and strongly-coupled MCFs. Weakly-coupled MCFs are the MCFs where the crosstalk between cores is well suppressed so that each core can be used as an isolated individual spatial channel and is compatible with conventional transceivers for SMFs. Strongly-coupled MCFs are the MCFs where crosstalk/coupling between cores is not negligible. There are no clear numerical criteria to distinguish weakly-coupled MCFs from strongly-coupled MCFs, and the same MCF may be a weakly-coupled MCF for (very) short-reach transmission and a strongly-coupled MCF for long-haul transmission. Weakly-coupled MCFs are often referred to as uncoupled MCFs or simply MCFs and strongly-coupled MCFs as coupled MCFs, coupled-core MCFs, or coupled-core fibers.

Strongly-coupled MCFs can be further divided into systematically-coupled MCFs and randomly-coupled MCFs [19]. Systematically-coupled MCFs are MCFs with the most strongly coupled cores. When multiple cores are located sufficiently close, the multiple cores act as a single microstructured multimode waveguide system. The eigenmodes of this coupled waveguide system can be approximated by the superpositions of the local modes of individual cores, hence called supermodes. In ideal waveguides, the supermodes are equivalent to the eigenmodes, hence orthogonal and uncoupled. For example, in a systematically-coupled MCF with two identical cores, when light is launched into the local mode of one core, the power of the light is sinusoidally transferred to and from the local mode of the other core due to systematic mode coupling. However, if we think of this behavior on a supermode basis, light is actually launched into both of the two eigenmodes (even and odd modes), and the sinusoidal power transfer between the cores is the beating between the uncoupled eigenmodes. In this article, we refer to the MCFs with uncoupled/weakly-coupled supermodes as systematically-coupled MCFs after the systematic mode coupling between the cores. By leveraging the weakly-coupled characteristics of the supermodes, the mode-division multiplexing using systematically-coupled MCFs has been proposed [32]–[34]. In actual systematically-coupled MCFs, various longitudinal perturbations can induce mode coupling between supermodes, but such a mode coupling can be suppressed by increasing the propagation constant mismatch between the supermodes, i.e., by increasing the mode coupling coefficient between the cores. Although the supermodes are weakly-coupled in systematically-coupled MCFs, splicing misalignment and mode field mismatch at the fiber input and output can easily induce the crosstalk between the supermodes. Therefore, the MIMO DSP is likely to be necessary for this type of MCF, especially for long-haul transmission.

Randomly-coupled MCFs are another type of strongly-coupled MCFs, which has coupling characteristics between that of systematically-coupled MCFs and weakly-coupled MCFs [35]–[37]. In this coupling regime, neither supermodes nor local modes stably propagate without modal coupling but the modes in randomly-coupled MCFs experience strong and random mode couplings along with propagation. Such randomly-coupled MCFs can be modeled as a concatenation of uncoupled short sections with strong and random mode couplings between adjacent sections, such as the fiber model in [23]. Strong and random mode couplings can make each section independent of adjacent sections. Thus, the standard deviation or root mean square (rms) of accumulated differential group delay (DGD) becomes square-root proportional

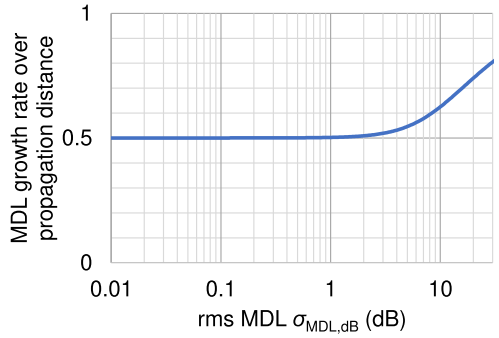

Fig. 1. *MDL growth rate in strong and random coupling regime. The MDL growth rate of 1 means linear proportion to propagation distance and 0.5 means square-root proportion.*

to the propagation distance. The rms MDL[1] σ_{MDL} of a randomly-coupled MCF system is also square-root proportional to the propagation distance, when rms MDL is less than 1 dB. To be precise, the rms MDL σ_{MDL} can be approximately expressed as [21]–[23][2]

$$\sigma_{\mathrm{MDL}} = \sqrt{\sigma_g^2 \frac{L}{L_c}} \sqrt{1 + \frac{1}{12(1-D^{-2})} \sigma_g^2 \frac{L}{L_c}} \tag{1}$$

$$\approx \sqrt{\sigma_g^2 \frac{L}{L_c}} \sqrt{1 + \frac{1}{12} \sigma_g^2 \frac{L}{L_c}} \tag{2}$$

where σ_g^2 is the variance of the MDL in uncoupled sections, L is the propagation distance, L_c is the coupling length[3], and D is the number of spatial and polarization modes. The MDLs σ_{MDL} and σ_g are expressed in units of natural logarithm of power gain, which can be converted to rms MDLs $\sigma_{\mathrm{MDL,dB}}$ and $\sigma_{g,\mathrm{dB}}$ in decibels by multiplying $10/\ln 10 \approx 4.34$, respectively. According to Ho and Kahn [21], [23], (2) is sufficiently accurate for practical purposes when $\sigma_{\mathrm{MDL,dB}} \leq 33$ dB for $D \geq 8$ (four cores or more). Fig. 1 shows the dependence of MDL growth rate on rms MDL, calculated based on (2). The proportionality of rms MDL to the propagation distance is sufficiently sublinear in a practical MDL range of less than 10 dB.

Although random coupling has to be compensated by MIMO DSP, the resultant properties, such as square-root/sublinear accumulations of MD and MDL, are beneficial to suppress the calculation complexity and outage probability of MIMO DSP [23], [38], [39].

[1]See Section IV-B1 for MDL definitions and [21] and [23] for further details.

[2]Different expressions for MDL accumulation were derived based on Stokes-space analysis and reported in [20], which are in square-root proportion to propagation distance regardless of the magnitude of the MDL value in contrast to (2). However, in both cases of [20] and [21]–[23], MDL in a practical range can be considered to be square-root proportional to the propagation distance.

[3]The number of fiber sections K in [21] and [23] is replaced by L/L_c in this article to explicitly show the MDL dependence on the propagation distance.

Table 1 Classification of MCF

Fiber type	Strongly-coupled MCF		Weakly-coupled MCF
	Systematically-coupled MCF	**Randomly-coupled MCF**	
Core pitch Λ	Small	**Medium**	Large
Mode coupling (crosstalk)	Weak between supermodes[a]	**Strong & random**	Weak between cores
Dominant source of MD, MDL	DGD, MDL between supermodes	**Both may affect**	DGD, MDL between cores
Proportionality of MD, MDL to propag. distance	Linear	**Square root (or sublinear)**	Linear

[a] Mode coupling between cores is strong and systematic (deterministic). So, we use the term "systematically-coupled" in this paper.

Table 1 summarizes the difference between randomly-coupled MCFs and the other types of MCFs.

III. FIBER DESIGNS

In this section, we briefly explain the design factors related to randomly-coupled MCFs and introduce typical examples.

Fig. 2 shows a summary of typical design parameters and properties. Randomly-coupled MCFs also have conventional design properties, such as attenuation, cutoff wavelength, and bending loss, which are designed or controlled by optimizing the refractive index profile of cores and cladding diameter in the same way as for SMFs, so they are not discussed in this article. Unlike weakly-coupled MCFs, intercore crosstalk suppression is not necessary for randomly-coupled MCFs, so one might consider that there is no need to optimize the core pitch Λ. However, as described in Section II, the pitch and layout of the cores are still important to assure random mode coupling.

Fig. 3 shows the simulated impulse responses of two-core fibers with different Λ's for a propagation distance L of 10 km. The two-core fibers are bent at a radius R of 140 mm and twisted at a rate γ of π rad/m, as schematically shown in Fig. 4 (see [18] for detailed calculation condition). When Λ is small (see Fig. 3, top) or large (see Fig. 3, bottom), the impulse responses have two peaks with a low-level plateau between them, such as the impulse responses of FMFs. This means that the propagation

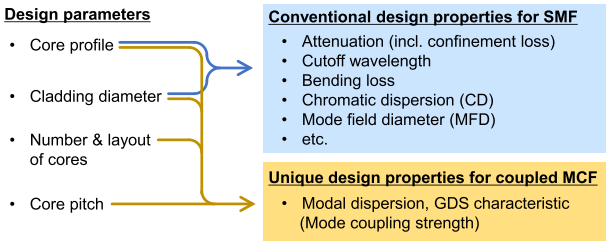

Fig. 2. *Summary of the design parameters and properties for coupled MCF.*

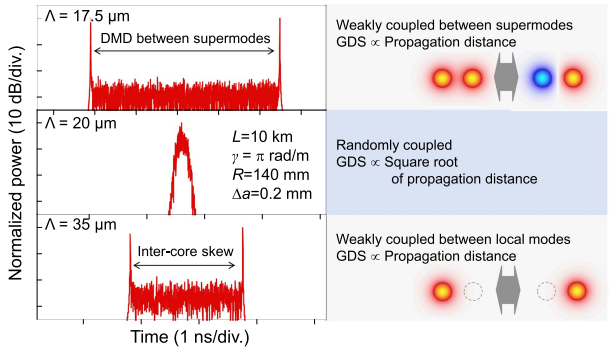

Fig. 3. *Numerically simulated impulse responses of two-core fibers with different core pitches.*

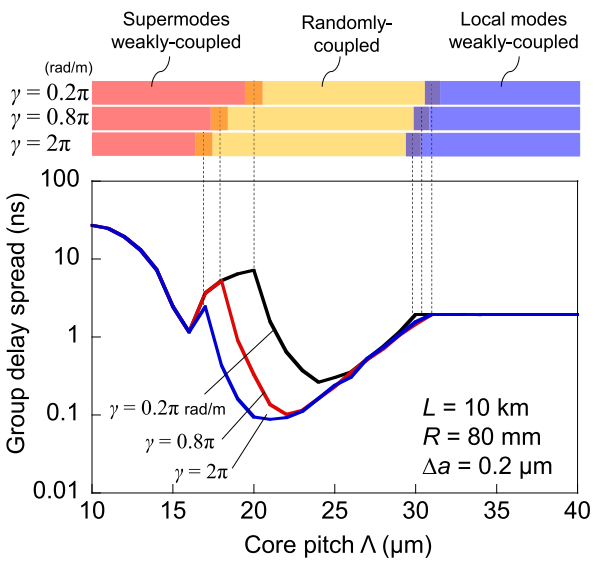

Fig. 5. *10-dB GDS width versus core pitch Λ for different γ's with schematic for illustrating Λ ranges corresponding to systematically-/randomly-/weakly-coupled MCFs.*

modes—supermodes or local modes—are weakly-coupled, and GDS increases in proportion to the propagation distance with a coefficient of differential mode delay (DMD) between supermodes or intercore skew due to manufacturing variation of refractive index profiles and bend-induced optical path length difference among local modes. The top and bottom examples correspond to systematically- and weakly-coupled MCFs, respectively. In contrast, the middle example in Fig. 3 shows an impulse response with Gaussian distribution, which is caused by random mode mixing realized at a Λ of around 20 μm [11], [18], [37]. In this case, the GDS increases in proportion to the square root of the propagation distance [16], [40], and thus, the GDS after long-distance transmission can be suppressed. Therefore, the core pitch Λ is an important design parameter to enhance random mode coupling.

External perturbations, such as fiber bends and twists, also affect random mode coupling and GDS [18], [19]. Fig. 5 shows the calculated GDS as a function of the core pitch for a 10-km-long two-core fiber at different γ's (see [18] for detailed calculation condition), where GDS is defined as a 10-dB down impulse response width. A core radius difference Δa of 0.2 μm was assumed since an MCF with perfectly identical cores is unrealistic, which induced flat GDS (intrinsic intercore skew) at $\Lambda \geq 30$ μm. As mentioned, the GDS can be suppressed thanks to random mode coupling in the appropriate Λ range, whereas too small/large Λ results in large GDS. Three bars at the top of the figure schematically indicate the Λ ranges where the propagation modes are weakly- or randomly-coupled. The interesting feature is that the optimum Λ range for random mode coupling depends on γ. This is because higher γ with fiber bends induces the steep change of eigenmode field profiles and enhances the coupling among them. It should be noted that other parameters, such as the refractive index profile, the number and layout of cores, and the fiber bend radius, also affect mode coupling strength and randomness. Thus, comprehensive design consideration taking into account external perturbation is necessary to control the MD of randomly-coupled MCFs. Various GDS simulation approaches have been proposed based on a constant/random bend orientation model with/without statistical R or γ distribution [18], [41], [42].

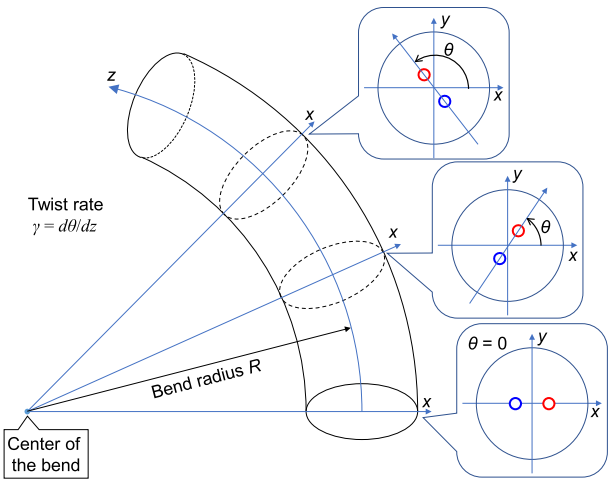

Fig. 4. *Schematic illustration of fiber bends and twists.*

So far, randomly-coupled MCFs with up to 12 cores have been reported. The characteristics and cross sections of major reported MCFs are summarized in Table 2 and shown in Fig. 6(a)–(f), respectively. Three-core fibers (3CFs) (first and second rows in Table 2) are the first reported randomly-coupled MCFs [14], [43], [44], and transmission of more than 4000 km was demonstrated [16], which showed the great potential of randomly-coupled MCFs for long-haul SDM transmission. Then, investigations on the MCF mode coupling mechanism revealed that the effects of fiber bends and twists

Table 2 Characteristics of Reported Randomly-Coupled MCFs

Core count	Attenuation[a] (dB/km)	A_{eff}[a,b] (μm^2)	λ_{cc} (μm)	Λ (μm)	Chrom. Disp.[a] (ps/(nm·km))	CD slope[a] (ps/(nm^2·km))	MD (SMD)[a] (ps/$km^{1/2}$)	Clad. diam. (μm)	Cross section	Refs.
3	0.177	104[c]	∼1.4[c]	38	21[c]	0.06[c]	n/a	125	[43]	[43], [44]
3	0.181	129[c]	∼1.35[c]	29.4	21[c]	0.06[c]	n/a	125	Fig. 6a	[14], [16]
3×3	∼0.19	56[c]	1.41[c]	22.3	19.9[c]	0.054[c]	n/a	143	Fig. 6b	[47]
6	0.236	106[c]	1.45[c]	28	20.6[c]	0.059[c]	n/a	125	Fig. 6c	[48]
4	0.155–0.160	111	1.47	20	20.0–20.1	0.060–0.063	6.1[d], 3.1[e]	125	Fig. 6d	[11], [12], [49]
7	0.171–0.172	112–114	≤1.50	23.5	21.1–21.4	0.06	22–28[d]	125	Fig. 6e	[24]
12	0.23–0.29	87[c]	1.31	16.4	19[c]	0.06[c]	8.4[d]	125	Fig. 6f	[13]

[a] Wavelength of 1550 nm. [b] Values of local modes. [c] Design values or calculated values. [d] R of 14 cm. [e] R of 31 cm.

on random mode coupling and MD must be considered for designing randomly-coupled MCFs [45], [46]. The MD also depends on the core arrangement [42].

For long-haul submarine transmissions, randomly-coupled four-core fiber with $\Lambda = 20$ μm (4C-MCF, fifth row in Table 2) and seven-core fiber with $\Lambda = 23.5$ μm (7C-MCF, sixth row in Table 2) were proposed [11], [24]. A core design based on an ultralow-loss silica-core SMF [50] realized an ultralow loss of 0.155 dB/km at 1550 nm [12] and properly designed core layouts realized suppressed spatial mode dispersion (SMD)[4] less than 30 ps/$km^{1/2}$. In particular, 4C-MCF achieved an SMD of 3–6 ps/$km^{1/2}$. The transmission experiments with 4C-MCF and 7C-MCF are described in Section VII. For telecom applications, randomly-coupled 12-core fiber with 125-μm cladding (12C-MCF, seventh row in Table 2) demonstrated an SMD less than 10 ps/$km^{1/2}$ by twisting the fiber to $\gamma = 4\pi$ rad/m during the fabrication process [13].

The right graph in Fig. 6 shows the relationship between the relative core density and the number of cores of reported randomly-coupled MCFs and also plots the results of weakly-coupled MCFs for comparison. Relative core density is defined as the number of cores per unit cross-sectional area, which is normalized by a standard 125-μm-cladding SMF. The marks on the dashed line correspond to MCFs with a 125-μm cladding. It is clear that randomly-coupled MCFs can achieve a higher core density than that of weakly-coupled MCFs owing to their smaller Λ design (typically 16–25 μm). One exception in the graph is the weakly-coupled seven-core fiber over the dashed line, but it is realized by small MFD cores to maximize spatial–spectral efficiency in weakly-coupled MCFs (i.e., aggregate spectral efficiency per cross-sectional area) [51]. Although the number of cores in randomly-coupled MCF should be carefully determined taking into account MIMO-DSP complexity, randomly-coupled MCFs can provide more than double the number of spatial channels compared to weakly-coupled MCFs in standard cladding design (typically with up to four cores for long-haul transmission in standard 125-μm cladding).

[4] See Section IV-B2 and Fig. 10 for the difference between MD and SMD.

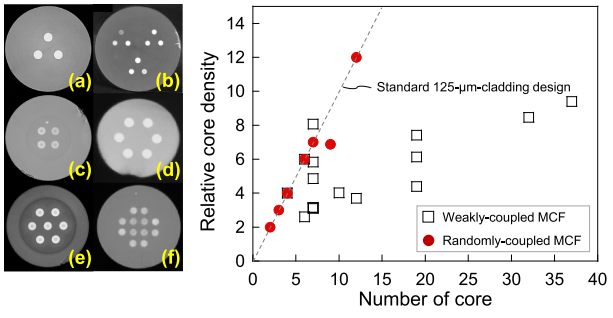

Fig. 6. *Left: cross sections of reported randomly-coupled MCFs—(a) 3CF [43], (b) 3 × 3CF with weakly-coupled three-core-groups where each core-group has randomly-coupled three cores, (c) four-core fiber [11], (d) six-core fiber [48], (e) seven-core fiber [24], and (f) 12-core fibers [13]. Right: relative core density versus the number of cores.*

IV. CHARACTERIZATION

A. Measurements of Mode-Averaged Characteristics

Since all modes in randomly-coupled MCFs are degenerated and randomly couple with each other along with fiber propagation, most of the optical characteristics, such as transmission loss, chromatic dispersion, and cutoff wavelength, can be measured as mode-averaged values using standard methods [52] with slightly modified fiber input and output. The difference between the modes can be evaluated as MD and MDL. This can be understood in analogy with the SMF, as we do not evaluate transmission loss, chromatic dispersion, and cutoff wavelength for individual polarizations but just evaluate them as polarization-averaged values. We evaluate polarization mode dispersion (PMD) and polarization-dependent loss (PDL) to determine the difference between two randomly-coupled polarization modes.

1) Transmission Loss Measurement: Transmission loss can be measured using standard measurement methods, such as the cutback technique and the backscattering technique [52]. Cutback measurement should be performed with single-mode input for suppressing higher order mode excitation and full mode reception of all the cores using a large-core multimode fiber (MMF) to avoid connection loss variation at the output [as shown in Fig. 7(a)]. Instead of using a receiving MMF, one can directly couple the

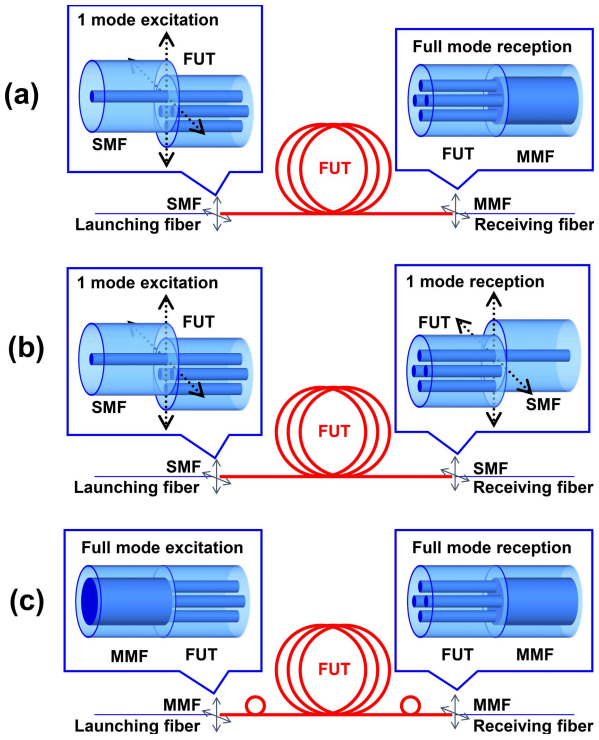

Fig. 7. *Schematics of the input and the output of light in randomly-coupled MCF measurements. (a) Single-mode excitation and full mode reception. (b) Single-mode excitation and reception. (c) Full mode excitation and reception. Instead of the MMF reception, one can directly couple the output end of the fiber under test (FUT) to a suitable PD in the full mode reception.*

output end of FUT to a suitable photo detector (PD) that can intercept all of the radiation emerging from the FUT. Though only one core is excited at the input, power will be fully mixed with the other cores within a short length of the FUT. The backscattering measurement can be performed with single-mode input [as shown in Fig. 7(b); the receiving fiber is not necessarily required in this measurement]. Measured backscattering loss traces will have an apparent point discontinuity at the input of the FUT as if connection loss between the launching fiber and the randomly-coupled N-core FUT was $10\log_{10} N$ dB because the input power to the one core of the FUT is immediately distributed to all of the N cores. After apparent point discontinuity at the input, the backscattering slope shows mode-averaged power attenuation under strong and random mode mixing after power coupling equilibrium.

2) Chromatic Dispersion Measurement: Chromatic dispersion can also be measured using standard measurement methods, such as the phase shift technique [52], [53] and the differential phase shift technique [53] with single-mode input and output, as shown in Fig. 7(b). Single-mode reception with a narrow linewidth (e.g., 10–100 kHz) light source may cause a fluctuation in measured group delay (GD), but a proper Sellmeier or polynomial fitting [52], [53] can be used for eliminating such a measurement noise [11]. A light source with a broader linewidth like 1–2 nm may help in the reduction of GD fluctuation, but the linewidth should be 10 nm or narrower [53] to suppress the wavelength averaging error on GD values.

3) Cutoff Wavelength Measurement: The cutoff wavelength can be measured using the standard transmitted power technique with multimode reference [52] with full-mode excitation and reception using MMFs with a large core covering all the modes of all the cores of the randomly-coupled MCFs, as shown in Fig. 7(c). Again, one can also directly couple the FUT to a PD, instead of using a receiving MMF. For randomly-coupled MCFs with single-mode cores, the cutoff wavelength can be defined as the wavelength at which the ratio of the total power, including higher order modes to the fundamental mode power, becomes 0.1 dB, as with the case of SMFs.

B. Measurements of Mode-Resolved Characteristics

1) Swept Wavelength Interferometry for MD/MDL Measurements: In order to fully characterize randomly-coupled MCF and associated components, the complex transfer matrix must be measured. This can be achieved using swept wavelength interferometry (SWI) [54], [55] for example. In contrast to estimating the transfer matrix from the DSP equalizer response [14], [16], [24], [48], SWI directly measures the transfer matrix by scanning laser and, therefore, allows for very broadband measurements in a single scan. One experimental setup for SWI-based characterization of randomly-coupled MCFs is shown in Fig. 8. A sweeping laser is split into two arms: one for the FUT and one for the reference arm. In the signal arm, before and after the FUT, relative delay fibers are used to time interleave the different elements of the transfer matrix and the two orthogonal launch polarizations. By using the input and output delays, the full transfer matrix can be measured in a single scan [56]. The length of the reference arm is chosen to be close, but not identical, to the shortest FUT length. After the FUT output delays, a polarization beam splitter is used to separate the two polarizations onto two different balanced photodiodes. The signal is then digitized and resampled to compensate for any laser sweep nonlinearities before the heterodyne beat notes matching the two polarizations for each core are extracted. To avoid

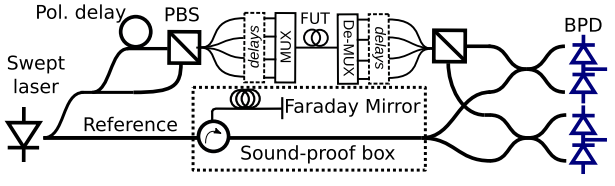

Fig. 8. *Experimental setup for full transfer matrix measurements of multiport devices using SWI.*

penalties from polarization rotations in the reference arm, especially for longer fiber length, such as the 69.2-km field-deployed randomly-coupled MCF (see Section V-D), a circulator and a Faraday rotator were used, as shown in Fig. 8. In addition, due to the interferometric nature of the SWI measurements, acoustic noise on the reference arm must be minimized. This is especially important with field-deployed fibers since the protected fibers in the ground often experience significantly less environmental noise compared to a reference spool placed in a laboratory. Susceptibility to environmental fluctuations can, furthermore, be minimized by using a fast-sweeping laser.

The full transfer matrix $\boldsymbol{H}(\omega)$ resolved with the angular frequency ω provides a full linear characterization of the system. From this matrix, effects such as frequency-dependence of the GDS and MDL can be quantified. The GDS can be found by analyzing the time-domain impulse response converted from $\boldsymbol{H}(\omega)$ or by evaluating the GDs of principal modes,[5] which are the imaginary parts of the eigenvalues of $[d\boldsymbol{H}(\omega)/d\omega]\boldsymbol{H}^{-1}(\omega)$ and also approximated by $\arg[\rho_m(\omega)]/\Delta\omega$, where ρ_m denotes the eigenvalue of principal mode m of $\boldsymbol{H}(\omega+\Delta\omega)\boldsymbol{H}^{-1}(\omega)$, with $\Delta\omega$ denoting the small enough ω step [59]. The MD may be defined as twice the standard deviation of the GDs of the principal modes over a given optical frequency range to be consistent with (rms) PMD definition[6] The peak-to-peak (P-P) MDL and rms MDL $\sigma_{\mathrm{MDL,dB}}$ in decibels for an D-mode system are defined according to

$$\mathrm{MDL_{P\text{-}P}}(\omega) = 10\log_{10}\frac{\max_i\left[|\lambda_i(\omega)|^2\right]}{\min_i\left[|\lambda_i(\omega)|^2\right]} \tag{3}$$

$$\sigma^2_{\mathrm{MDL,dB}} = \mathrm{E}\left\{\left[10\log_{10}|\lambda_i|^2 - \mathrm{E}\left(10\log_{10}|\lambda_j|^2\right)\right]^2\right\} \tag{4}$$

respectively, with λ_i denoting the singular values of the transfer matrix $\boldsymbol{H}$ and the operator E denoting the expected value. Note that, in the case of $D = 2$, corresponding to a dual-polarization single-mode signal, the MDL is equivalent to the PDL. We, furthermore, note that, while the transfer matrix can also be accurately measured using DSP, enabling estimation of both MD and MDL, SWI benefits from improved signal-to-noise ratio (SNR) due to the narrow bandwidth signals compatible with lower speed higher resolution electronics, and the bandwidth from a laser sweep can easily cover multiple terahertz.

2) Intensity-Based MD Measurement: MD can be measured also using the fixed analyzer (FA) method [61] with modified input and output [18], which only requires intensity measurement without phase-sensitive detectors. The FA method was originally developed for PMD measurement of SMFs. In a PMD measurement, as shown in Fig. 9(a), the transmission spectrum of a polarization channel of an SMF is observed with linearly polarized input and output with arbitrary but "fixed" polarization angles. Then, the transmission spectrum is (inverse) Fourier transformed to the ACF of the impulse response of the polarization channel [60] based on the Wiener–Khinchin theorem. The envelope of the ACF corresponds to the probability distribution of the DGD of polarization modes. Under random polarization coupling, the shape of the ACF envelope becomes Gaussian. The standard deviation σ, or the square root of the second moment, of the ACF is defined as the PMD, which is twice the standard deviation of the impulse response [60].

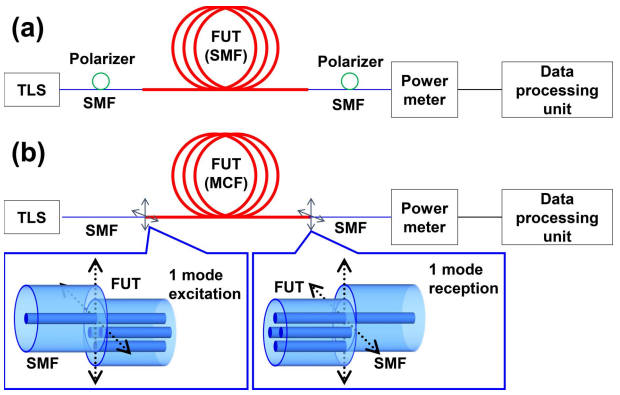

Fig. 9. *Setup for (a) PMD or (b) SMD measurement. (TLS: tunable light source.)*

As well as the SMF, the MD of randomly-coupled MCFs can be measured using the FA method by modifying the input and the output. Fig. 9(b) shows a measurement setup for "SMD" of a randomly-coupled MCF. This configuration is almost the same as that for PMD measurement, but single-mode input and output are employed for analyzing the interference pattern of a spatial channel with the input and the output of arbitrary but fixed spatial mode states. Since SMD is more than one order of magnitude larger than PMD, we can omit the two polarizers and define the *SMD* as the standard deviation of the ACF of the spatial channel evaluated with a polarization-insensitive analyzer [18]. To be rigorous, one can use a linearly polarized light source and polarization-sensitive analyzer with the setup in Fig. 9(b) to analyze the interference pattern with arbitrary but fixed polarization and spatial mode states at the input and the output, and evaluate the *MD* among polarization and spatial modes. Fig. 10 briefly summarizes the difference between these MDs.

Fig. 11 shows examples of an FA measurement recorded with randomly-coupled two-core fibers and its Fourier transform or the DGD distribution [18]. The DGD is Gaussian distributed, which is similar to that of SMFs with random polarization coupling. The standard deviation of the DGD σ_τ is square-root proportional to the propagation distance, as already discussed in Sections II and III, so the SMD coefficient is often expressed with a unit of

[5]In analogy to principal states of polarization [57], the modal shapes of the uncoupled orthogonal channel bases of the system with multiple spatial modes are referred to as "principal modes [58]."

[6]Twice the standard deviation of an intensity impulse response or the standard deviation of the autocorrelation function (ACF) of the intensity impulse response [60].

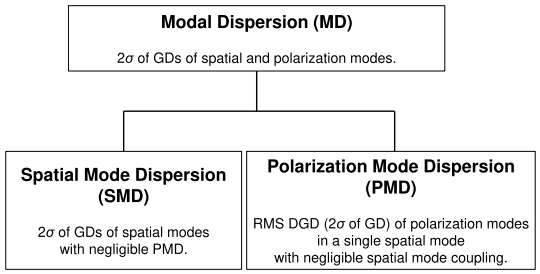

Fig. 10. *Classification of MDs.*

ps/km$^{1/2}$, such as the PMD of SMFs. It has been reported that the variation among SMD coefficients measured by different input–output core combinations was negligible for randomly-coupled MCFs [13]. The FA measurement is scalable for MCFs with more than two cores, and the results for MCFs with up to 12 cores have been reported so far [11], [13], [18].

3) Intensity-Based MDL Measurement: MDL can also be measured with an intensity measurement without a phase-sensitive detector [62], [63]. One of the easiest measurement methods is the scrambling method [63], whose measurement setup is shown in Fig. 12. In the scrambling method, the modal state of the light is scrambled at the input of the FUT, and the whole output power of the FUT is measured using a PD. The whole output power is fluctuated by modal state scrambling at the input or modal state scrambling over propagation. The standard deviation of the whole output power fluctuation is approximately equivalent to the rms MDL expressed in (4) [63] for low MDL cases. Although realizing a low-MDL spatial and polarization mode scrambler is not easy, wavelength scanning with a narrow linewidth tunable light source (TLS) can sufficiently scramble the modal state in a randomly-coupled MCF over propagation. To achieve sufficient scrambling, the wavelength scanning range should be sufficiently wider than the spectral correlation width of the transfer matrix. In [63], a TLS with a 20-kHz linewidth was

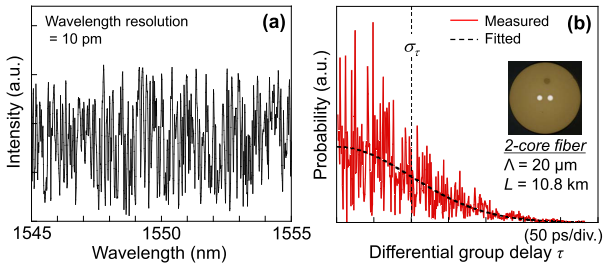

Fig. 11. *Example of (a) FA measurement (transmission spectrum of single-core input and single-core output) and (b) its Fourier transform (DGD distribution) obtained from 10.8-km-long two-core fiber with a core pitch of 20 μm using the setup shown in Fig. 9(b). (Replotted from the data in [18].)*

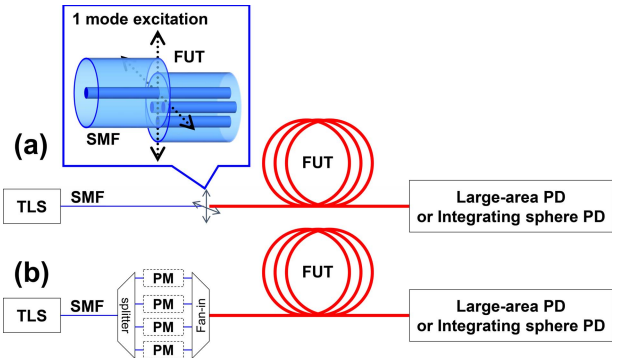

Fig. 12. *MDL measurement setup of the scrambling method. (a) Single-mode excitation. (b) All-mode excitation with additional phase scrambling. (TLS: tunable light source and PM: phase modulator.)*

swept over 1550 ± 1 nm at a rate of 0.5 nm/s, and phase scrambling of each spatial channel was also employed to enhance scrambling of the modal state, as shown in Fig. 12(b).

C. Measurements of Field Profiles

1) Mode Basis for Field Profile Measurement: The modes in randomly-coupled MCFs can be represented by various mode bases, such as the local modes and the eigenmodes. The eigenmodes are the true orthogonal fiber modes, but the field profiles of the eigenmodes of randomly-coupled MCFs are heavily dependent on external perturbations, such as fiber bends and twists [18], [19]. Thus, the eigenmode profiles after fiber deployment are difficult to predict from fiber spool measurements. In contrast, local modes are solely dependent on the refractive index profiles of the individual cores and almost independent of external perturbations (to be precise, local mode profiles are affected by bend-induced perturbations, but the effect is negligible for splice loss performance and the nonlinearity of installed fibers). Thus, local mode profiles are suitable for use in evaluating optical fiber performance. Either mode basis, local mode or eigenmode, is legitimate for simulating nonlinear propagation in randomly-coupled MCFs [64] and can be converted to the other basis by unitary rotation with fiber bend and twist information [18], [19].

2) Low Coherence Method for Stable Field Profile Measurement: To evaluate the mode-field diameter and the effective area (A_{eff}), data for the far-field profile (FFP) and near-field profile (NFP) are necessary. In SMF measurements, the FFP can be measured using the far-field scan (FFS) method [52], and the NFP is accurately converted from the FFP using the Hankel transform [61]. Alternatively, the NFP can be measured directly using magnifying optics, but various items should be taken into consideration in order to realize high accuracies, such as selection of the numerical aperture and magnification of the optics, calibration of the magnifying optics, and

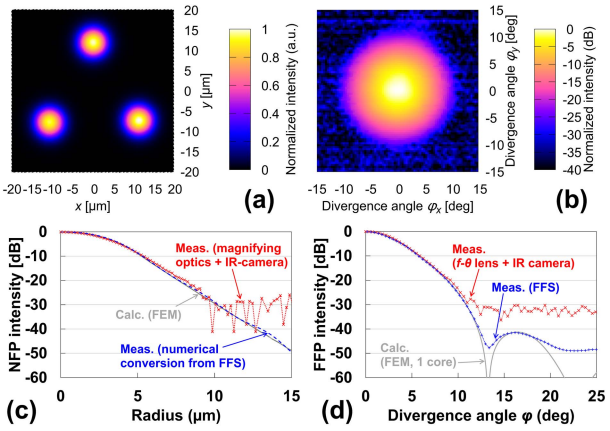

Fig. 13. *NFP and FFP of a 3CF measured by the low-coherence method: 2-D profiles of (a) NFP and (b) FFP recorded using IR camera and lens systems [49], and 1-D profiles of (c) NFP of a core of the 3CF and (d) FFP of the 3CF [65]. (FFS: far-field scan and FEM: finite element method.)*

focusing with maximum accuracy to reduce dimensional errors [52].

Typically, the field profile of an SMF is measured using a short fiber sample and a narrow-linewidth light source; however, when we observe the field profiles of randomly-coupled MCFs in this way, the field profile fluctuates due to the interference between multiple optical paths that varies with time (and wavelength) because of random mode coupling. Such an intensity fluctuation can be understood as a moving interference fringe and can be suppressed by reducing the degree of coherence, which can be achieved by increasing the linewidth of the light source and/or by increasing the optical path length difference between the interfering light components. Therefore, the randomly-coupled MCF output field can be stably measured by simply using a long randomly-coupled MCF sample and a broadband light source [49], [65]. The intensity variation of randomly-coupled MCF output is approximately inversely proportional to the product of the bandwidth of the light source and the MD, and intensity variation can be suppressed to less than 1% when the product of $1/e$ bandwidth and MD is more than 45 when the light source has a Gaussian spectrum shape.

Fig. 13 shows an NFP and FFP obtained using the low coherence method. The NFP directly measured with magnifying optics and an infrared (IR) camera shows very straightforward results with three isolated peaks corresponding to the individual cores. On the other hand, the FFP measured with the low coherence method becomes the average (or sum) of the FFPs of each core. This is because the NFP and FFP are a Fourier transform pair, and the positional displacement of each core in the NFP just tilts the phase in the FFP and does not change the amplitude or intensity. Thus, the incoherent superposition of the FFPs of multiple cores is just the sum of the FFPs of the cores. Therefore, one can measure the *average* MFD and A_{eff} from an FFP measurement with the low-coherence method.

In summary, the low coherence method can stabilize the measurement results of the NFP and FFP of randomly-coupled MCFs. The direct measurement of the NFP can provide information on the cores individually, but the spatial resolution and dynamic range may be limited by the magnifying optics and IR camera [see Fig. 13(c)]. Thus, the evaluated MFD and A_{eff} might have larger errors. In contrast, the FFP measurement can only provide the *average* profile of the cores but can achieve higher spatial resolution and dynamic range [see Fig. 13(c) and (d)] so that the evaluated MFD and A_{eff} can achieve better accuracy.

V. CONNECTIVITY, CABLING, AND DEPLOYMENTS

A. Splicing Characteristics

Randomly-coupled MCFs have better splicing performance compared to weakly-coupled MCFs since the cores of randomly-coupled MCFs can have larger MFDs and/or closer positions to the cladding center. Fig. 14 shows the splice loss characteristics of the 4C-MCF with local-mode MFD of $\sim$11 μm [see Fig. 6(c)]. Splice loss can be suppressed to as low as 0.02 dB with rotational misalignment of 1° or smaller [66], where a minimum splice loss of 0.02 dB is considered to be caused by tilt misalignment due to cleave angle imperfection and fusion-induced waveguide deformation. Even with a large rotational misalignment, the so-called thermal expanded core (TEC) technique can reduce the splicing loss of randomly-coupled MCFs.

Compared with FMFs, randomly-coupled MCFs have been reported to have better MDL characteristics at splice points. In FMF splicing, lateral offset causes MDL because the higher order modes have field profiles that significantly differ from each other. On the other hand, the modes of randomly-coupled MCFs have field profiles similar to each other in intensity either on a local mode or supermode basis; thus, MDL due to splicing is expected to be much smaller than that for FMF. Spliced-induced MDL has been numerically and experimentally investigated for the 12C-MCF [see Fig. 6(f)] and a single-core ten-mode fiber [67] and showed that MDL caused by axial misalignment in the 12C-MCF can be suppressed to about 1/5 of

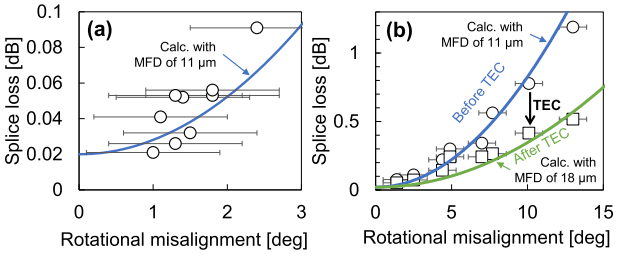

Fig. 14. *(a) Splice loss with rotational misalignment. (b) Splice loss reduction through the TEC treatment. (Replotted from the data in [66].)*

that in the ten-mode single-core fiber. Experimental MDL measurements on the 4C-MCF demonstrated that, under lateral misalignment, the splice-induced rms MDL increase is 1/10 of the splice loss increase [63]. Since the splice loss of the 4C-MCF can be very low as mentioned above, the splice-induced MDL of this type of randomly-coupled MCFs can be negligibly low. Further studies on various types of randomly-coupled MCFs with various core pitches with multiple splice points are expected to elucidate more details of the splicing MDL characteristics of randomly-coupled MCFs.

B. Fan-In/Fan-Out

Fan-in/fan-out (FIFO) devices provide the access to MCF cores from corresponding SMFs (see [68] for detailed review). The FIFOs for randomly-coupled MCFs must have shorter Λ at the interface for an MCF compared to those for weakly-coupled MCFs; therefore, suitable technology for FIFOs will differ.

A laser-inscribed 3-D waveguide [47], [48], [69] is one option that can realize short Λ at the MCF interface, but the reduction of insertion loss is a challenge because of the surface roughness of a waveguide inscribed by laser pulse repetition. A fused taper type FIFO is also a suitable technology for randomly-coupled MCFs [24], [70], [71]. In [71], four-core FIFOs were fabricated by tapering down the assembly of four strands of 125-μm-cladding 6-LP-mode fibers inserted into a four-hole fluorine-doped glass capillary. The loss for the fabricated FIFOs was less than 0.1 dB, but splicing to the randomly-coupled MCFs increased the loss to 0.4–0.5 dB, probably due to the mode field mismatch at the MCF end and SMF end. Further low insertion loss is expected by properly designing the fibers and capillary to assure adiabatic tapering and mode field matching at the input and the output. Free space optics can also be used for the FIFOs for randomly-coupled MCFs [28], and a low insertion loss below 0.5 dB is achievable [72], [73]. Another good point of free space optics is that they can integrate other functions, such as an optical isolator and a tap monitor [74]–[77]. Fused taper type and free space optics type FIFOs are free from the adhesive on light paths and, thus, good candidates for the FIFOs used in submarine systems that require high reliability for long period.

The etched fiber bundle type of FIFO is often used for weakly-coupled MCFs [78] but is not suitable for randomly-coupled MCFs because the SMFs for the FIFO have to be etched down to a very thin diameter to match Λ of randomly-coupled MCFs. Very thin fibers are difficult to handle and sensitive to the losses induced by microbends and tunneling to surrounding materials, such as adhesive and capillary.

C. High-Density Ribbon Cable With Controlled SMD

Since the SMD of randomly-coupled MCFs highly depends on fiber bends and twists, it is preferable to control them through cable design. Not only for randomly-coupled MCF cables but also for conventional high-density SMF cables, fiber bends and twists in cables are an important design consideration. In high-density SMF cables, the optical fibers are bundled for ease of identification and manufacturing, and stranded to ensure bending strain characteristics and for ease of optical fiber extraction from the cable [79].

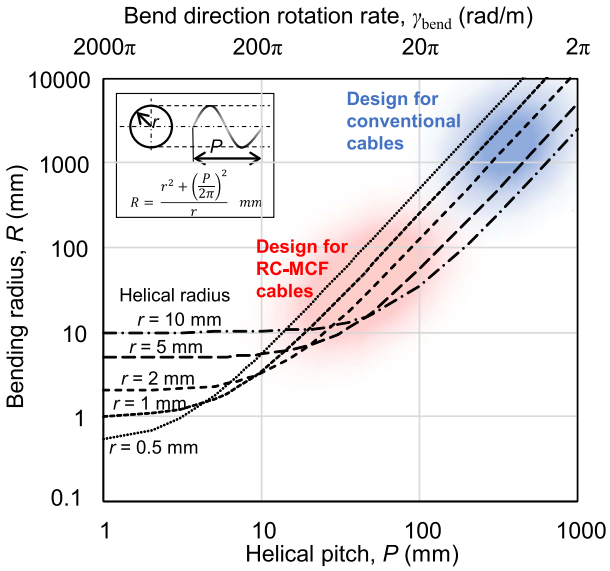

Fig. 15. *Relationship between fiber bending radius and rotation rate of fiber bend direction in the cable and cable design parameters.*

The optical fibers in the stranded structure are deformed in a helical shape, and the helical radius r and the helical pitch P determine the fiber deformation (bend radius R and bend direction rotation rate γ_{bend}). The bend direction rotations perturb the modes along with the fiber as is the case with fiber twists under a fixed bend direction. Thus, one can virtually control the bends and twists of the fibers in the cable by controlling cabling parameters, such as P, as shown in Fig. 15. The helical pitch P of a conventional optical cable is several hundred millimeters or more, but shorter P is preferable for enhancing random coupling with smaller R and higher γ_{bend}. The SMD coefficients of randomly-coupled MCFs can be controlled by properly designing optical cabling parameters. A method for controlling fiber bending in a high-density optical cable was proposed in [80], which is schematically shown in Fig. 16. Fig. 16(a) shows a cross section of a 200-fiber cable. This cable is composed of 54-fiber partially bonded rollable ribbons, strength members, rip cords, and a polyethylene sheath. The cable has ten fiber units containing five rollable optical fiber ribbons, and the fiber units are stranded with each other. Fig. 16(b) shows a longitudinal image of a fiber unit, which is bundled with tape as shown by the red line. By winding the bundle tape around the fiber unit

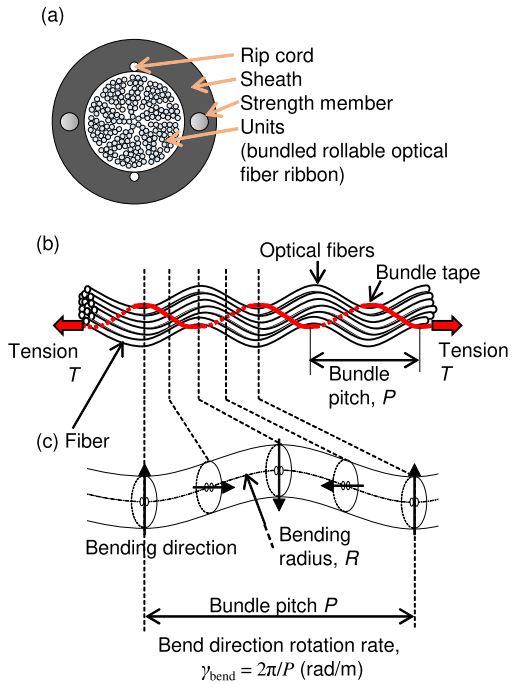

Fig. 16. *Configuration of a cable for controlling fiber bend radius and bend direction rotation. (a) Configuration of cable. (b) Bundled fiber unit. (c) Fiber.*

with bundle pitch P and tension T, the bundled optical fibers in the fiber unit are deformed into a helical shape, as schematically shown in Fig. 16(c). This deformation enables changes to the bending radius R and the bend direction rotation rate γ_{bend}. As a result, the SMD coefficient can be controlled in a high-density optical cable by optimizing P and T. This method only requires changes to the tension and pitch of the bundle tape without major changes to the optical cable assembly method. Bending can be applied to each unit regardless of the number of fibers in the optical cable.

The optical characteristics of randomly-coupled MCFs cabled by controlling cable parameters have also been reported. The cabled randomly-coupled MCF had two cores with a Λ of 20 μm. Each core of the randomly-coupled MCF had a step index profile, and the cutoff wavelength was 1435 nm. It was verified that the proposed cable (relative tension $T = 1$) could reduce the SMD coefficient by 47% compared with conventional cable (relative tension $T < 0.3$) while retaining an acceptable cabling loss increase. Simultaneous optimization of both randomly-coupled MCF and cable parameters can be expected to improve characteristics, such as expanding the number of cores and mitigating the tradeoff between optical loss and SMD in cables.

D. Loose-Tube Cable Deployments

Loose-tube optical fiber cable is another type of optical fiber cable. A variety of loose-tube cables are widely used, such as indoor cords, outside plant cables, and submarine optical fiber cables.

An indoor round cord with randomly-coupled MCFs was fabricated for investigating the relationship between the SMD and Λ [81]. The experiments and simulations found that a randomly-coupled MCF with a proper core pitch has random mode mixing even in the straightened loose-tube cable, and random fiber deformation due to slight extra fiber length in the loose-tube cable can introduce sufficient bends to randomly-coupled MCFs for inducing random mode coupling.

In 2019, an MCF cable was deployed in the city of L'Aquila, Italy, as the world's first field-deployed testbed for SDM fibers [82], as shown in Fig. 17. The deployed cable was a 6.29-km jelly-filled loose-tube cable with an outer diameter of 6 mm, shown in Fig. 18(a), which accommodates 18 MCFs in total and consists of 12 strands of randomly-coupled MCF and six strands of weakly-coupled MCFs. The randomly-coupled MCFs have four identical cores with a square layout of 25.4-μm pitch and a cladding diameter of 125 μm, whose cross section is shown in Fig. 18(b) and the optical properties of which are summarized in Table 3.

One strand of the randomly-coupled MCF was terminated by splicing SC-connectorized MCF pigtails on both ends, which can be connected to FIFO devices with connectorized MCF pigtails. The remaining 11 strands of randomly-coupled MCF were spliced with each other to configure a concatenated randomly-coupled MCF link with

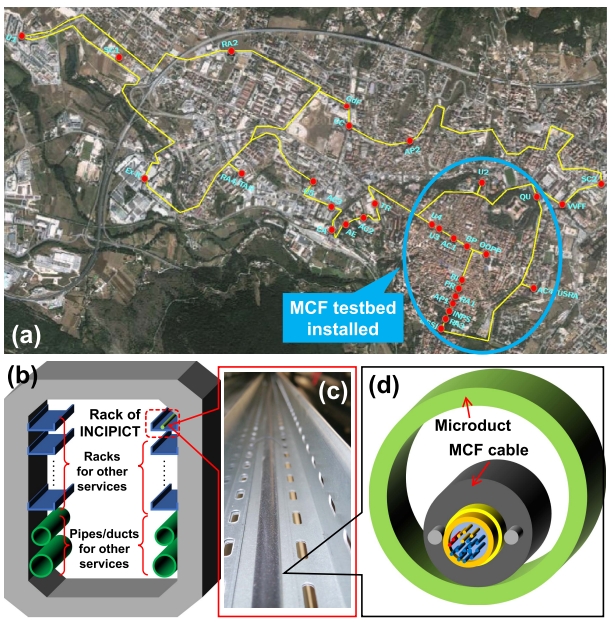

Fig. 17. *Field-deployed MCF cable testbed [82]. (a) Experimental optical network of the INCIPICT [83] and the MCF cable installation area, (b) schematic of the underground tunnel with the INCIPICT rack, (c) microduct on the rack after the MCF cable installation, and (d) schematic of the MCF cable installed in the microduct.*

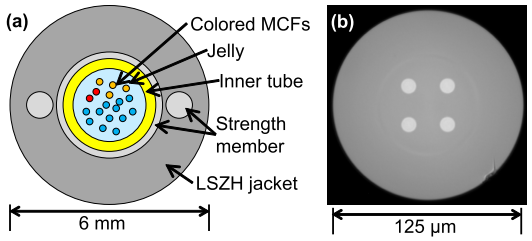

Fig. 18. *Cross sections of the field-deployed (a) loose-tube cable and (b) randomly-coupled MCF [82]. (LSZH: low smoke zero halogen.)*

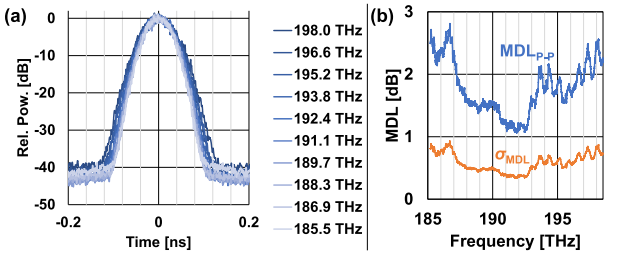

Fig. 19. *(a) Impulse response at various center frequencies for the 69.2-km-long coupled-core MCF. (b) Corresponding MDL data. (Replotted from the data in [55].)*

a length of 69.2 km that can be used for long-distance recirculating loop transmission experiments. Both ends of the concatenated randomly-coupled MCF link were spliced directly to the MCF pigtails of a pair of MCF FIFO. The splicing loss of the ten splice points between the 11 randomly-coupled MCF strands (except both ends of the link) was measured at 0.12 dB/splice on average using OTDR, which can be further improved by optimizing splicing conditions. Fiber transmission loss, including splicing loss, can be regarded as 0.187 dB/km (0.170 dB/km + 0.12 dB/splice × 10 splices/69.2 km) at 1550 nm. The SMD of the link measured using the FA method was 47 ps after a 69.2-km transmission (5.7 ps/km$^{1/2}$), which is consistent with the rms value (5.1 ps/km$^{1/2}$) of the SMDs of the 11 randomly-coupled MCF strands composing the concatenated link.

The impulse response for the 69.2-km-long randomly-coupled MCF measured using SWI is shown in Fig. 19(a). We observe a bell-shaped response confined to within ±0.1 ns, and the absence of any peaks or other nonsmooth features verifies the high quality of both the fiber and the fan-in/fan-out. The impulse responses had 2σ of 44–55 ps in the range of 185.5–198.0 THz (i.e., 1616–1514 nm), which are in good agreement with the SMD of 47 ps measured in the FA method. The corresponding MDL measurements are shown in Fig. 19(b). The rms MDL stayed below 1 dB over the >12-THz measurement bandwidth, with a minimum of about 0.35 dB observed between 191 and 193 THz, and the P-P MDL below 3 dB with a minimum of about 1.1 dB. The ratio of P-P MDL to rms MDL was 3.07 ± 0.08 in the whole measurement frequency range. These values are directly comparable with the MDL estimates from the estimated transfer matrix using DSP. Worth noting is that at least part of the MDL increase at longer and shorter wavelengths is likely due to calibration issues with the broadband SWI system. Nevertheless, the low MDL values measured for the field-deployed randomly-coupled MCFs verify that MDL levels reported in laboratory experiments are achievable also for the deployed randomly-coupled MCF.

Transmission experiments were conducted over the field-deployed randomly-coupled MCF link, and the recirculating loop experiments achieved the successful transmission over distances up to 4014 km for QPSK and 2768 km for 16QAM signals with off-line DSP [84]. Furthermore, real-time MIMO DSP implementation revealed that the channel dynamics of the field-deployed randomly-coupled MCF are richer than SMF but still significantly slower than the update speed of the real-time DSP [85], [86]. The results confirmed the technical viability of randomly-coupled MCFs in the field.

Table 3 Optical Properties of the Field-Deployed Randomly-Coupled MCFs

Attenuation [dB/km]	0.170 (0.165–0.175)[a,b]
A_{eff} [μm^2]	80.9±3.3[a]
MFD [μm]	10.1±0.2[a]
Cutoff wavelength [μm]	1.47–1.50
Chromatic Dispersion [ps/(nm·km)]	19.1[a]
CD slope [ps/(nm^2·km)]	0.058[a]
SMD over C-band [ps/km$^{1/2}$]	5.2 (2.5–8.0)[c]

[a] Values at the wavelength of 1550 nm.
[b] Avg. (min.–max.). [c] RMS (min.–max.).

VI. COUPLED MULTI-CORE AMPLIFIERS

A single multi-core erbium-doped fiber amplifier (EDFA) [87]–[89] can amplify all the parallel spatial channels in a more compact footprint compared to simply duplicating SMF-based EDFAs. Due to the availability of uncooled high-power multimode pump laser diodes and their potential to lower the cost per bit and total power consumption, cladding pumping schemes, such as edge [89], [90] and side pumping [88], are adapted and commonly applied in multi-core EDFAs. In cladding pumping, pump light is distributed over the entire cladding, but signal light only transmits inside the cores. The small overlap between the pump and signal results in a much lower pump absorption efficiency compared to core-pumped EDFA. A large portion of the pump light is usually unused and dumped at the amplifier output in order to maintain high population inversion over the entire EDFA for better performance, such as a low noise figure [88]. Potential pump absorption efficiency enhancement can be achieved by increasing core and cladding area ratio [91] and implementing pump recycling [92].

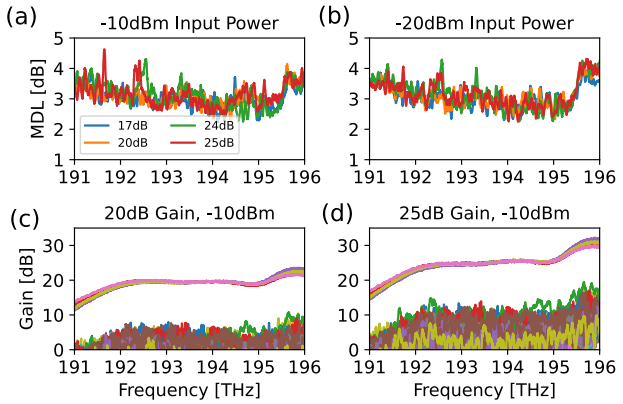

Fig. 20. *Measured P-P MDL and gain for a packaged randomly-coupled seven-core EDFA using all seven-core components [95]: (a) and (b) P-P MDL after pump optimization for various input power level (top of each graph) and gain [legend in (a)], and (c) and (d) corresponding gain flatness for 20-/25-dB target gain at −10-dBm input. The amplifier was loaded using a 40 DFB lasers on a 100-GHz grid.*

Core-pumped multi-core EDFAs can achieve the same pump absorption efficiency as in conventional SMF-based EDFAs. Fiber cores can be designed to the couple at both signal and pump wavelengths for reducing mode-dependent gain by scrambling the signals, balancing the pump power across all the cores, and reducing the required number of pump laser diodes [93]. State-of-the-art core-pumped coupled-core EDFAs can achieve more than a 15-dB gain and a noise figure of less than 5 dB [94]. Fig. 20 shows the measured results of a packaged randomly-coupled seven-core EDFA, which achieves less than 3-dB P-P MDL (estimated to be <1-dB rms MDL) while offering more than 25-dB gain [95]. The MDL suppression of multi-core EDFA is a remaining challenge for realizing long-haul all MCF transmission links [25], [96], but the MDL caused by multi-core EDFAs is expected to be further suppressed by the MDL suppression of coupling subcomponents and optimizing the coupling strength among the cores.

VII. TRANSMISSIONS AND SYSTEMS

Randomly-coupled MCFs are very attractive for high-spatial density high-capacity optical transmission applications due to their favorable optical properties like low loss and small SMD compared to other fibers supporting multiple spatial channels, for example, graded-index MMFs. This was confirmed by numerous MIMO-based transmission experiments performed over the last decade [14], [16], [24], [28]–[31], [43].

The work in [24] is of particular importance because it reports a direct comparison of an SMF (ULA-SMF) with randomly-coupled four-core fiber (4C-MCF) and seven-core MCF (7C-MCF) with nominally identical core design, measured in the same recirculating loop setup. The results are reported in Fig. 21, measured using 15-channel WDM signals modulated with 30-Gbaud QPSK and 16QAM signals. In the experiments, the span length was 110 km, and the fiber attenuation per span was 17.6 dB for ULA-SMF, 17.5 dB for 4C-MCF, and 18.9 dB for 7C-MCF at a wavelength of 1550 nm. Fused taper type FIFO devices were fabricated for the 4C-MCF and 7C-MCF, and FIFO loss was 0.4–0.5 dB for the four-core FIFO and 1 dB for the seven-core FIFO, which includes the splice loss between the FIFOs and MCFs. The effect of the FIFO losses was eliminated from the launch power in Fig. 21(a), so the launch power is the power in the fibers.

Although the randomly-coupled MCFs, especially the 7C-MCF, were penalized by additional span loss, the reported quality factors (Q-factors) Q^2—calculated from bit-error-rate measurements—clearly show that the randomly-coupled MCFs can outperform the SMF performance for an equivalent core design with nominally the same index profile [11]. The effect was predicted in [27], [97], and [98] and can qualitatively be explained by the favorable averaging between the nonlinear distortions contributions arising from the nonlinear interactions between the spatial modes.

The improvement in nonlinear transmission resulting from having multiple randomly-coupled cores in an MCF has been numerically evaluated in [99]. Fig. 22(a) shows Q-factors versus power per channel for the central channel of a 15-channel signal and for two, four, seven, and 19 identical randomly-coupled cores with a coupling length of 200 m that represents the distance over which the signal mixes from the random linear coupling. The performance of one core is shown as a reference. One can see that, as the number of coupled cores grows, the Q-factor improvement of MCF over one core increases but appears to experience saturation. The "ideal" curve represents ideal modulation and detection in the presence of noise only.

The effect of the coupling length on nonlinear transmission for a four-core randomly-coupled MCF is displayed in Fig. 22(b). The coupling length of ∞ represents the reference case of a single-core fiber. The Q-factor improves as the coupling length decreases from 2 km to about 2 m, with the most significant gain experienced when the coupling length is reduced to a few hundreds of meters. The improvement in nonlinear transmission appears to saturate when the coupling length further decreases to a distance as short as a few meters. Fig. 22 shows that the improvement in nonlinear transmission originates from the random linear coupling alone and is in addition to any other gain in nonlinear transmission, such as an increase in the effective area. One should note that there are limitations in reducing the coupling length by bringing the cores closer when the propagation constant of the modes supported by the MCFs starts to no longer be considered degenerate, as mentioned in Sections II and III. The modeling of randomly-coupled MCFs within the limit of short coupling length can be performed using a set of averaged coupled differential equations, referred to as generalized Manakov equations [100], [101].

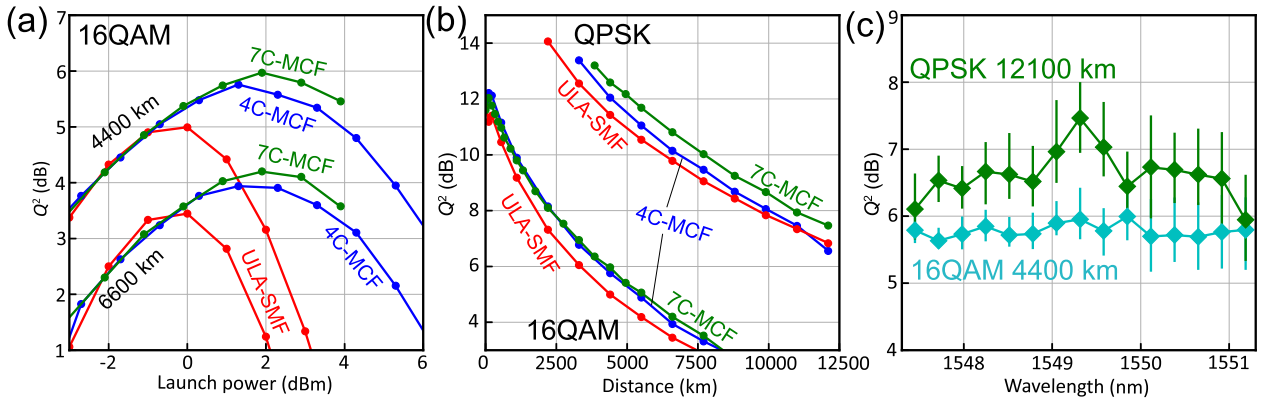

Fig. 21. *Q-factors for ultralow-loss large-effective-area SMF (ULA-SMF), 4C-MCF, and 7C-MCF as a function of (a) launch power (16 QAM) and (b) distance (QPSK and 16QAM). For 7C-MCF, (c) Q-factor as function of wavelength channel for a transmission distance of 4400 (16QAM) and 12 100 km (QPSK) [24].*

The impulse responses of the 4C-MCF and 7C-MCF loops are reported in Fig. 23(a) for a distance of 2200 km. The 20-dB impulse widths were 2.6 ns for the 4C-MCF and 5.6 ns for the 7C-MCF, which are significantly shorter than DMD observed in MMF transmissions over the same distance [102]. Since the total impulse response width is the root sum square of the impulse response widths of individual components, 0.87 ns comes from the transmission fiber and 2.5 ns from the other (loop) components in the 4C-MCF loop, and 3.6 ns from the transmission fiber and 4.2 ns from the other (loop) components in the 7C-MCF loop, for a distance of 2200 km. The width of the impulse response has a direct impact on the number of equalizer taps necessary to fully recover the signal. For the signal at 30 Gbaud transmitted over the 7C-MCF loop, 170 symbol spaced taps are required at a distance of 2200 km, and 356 taps are required for distances up to 10 000 km. MIMO equalizers with such a number of taps are best implemented using frequency-domain equalizers that scale more favorably than time-domain equalizers. In addition, the complexity can also be reduced by using digital subcarrier modulation, practically reducing the symbol rate of the transmitted subcarrier, which results in a smaller number of taps that have to be optimized for each subcarrier [103]. The evolution of the MDL as a function of the distance was also investigated, as it can have a significant impact on the transmitted capacity [104]. The results are shown in Fig. 23(b) where the MDL defined in (3) is reported, as well as the standard deviation defined in (4), which is relevant for strongly coupled systems [21]. The measurements of $\sigma_{\mathrm{MDL,dB}}$ agree well with the theoretical prediction (2) from [21] when a value of $\sigma_{g,\mathrm{dB}} = 0.30$ dB is used for the per span $\sigma_{\mathrm{MDL,dB}}$ of the 7C-MCF, which is lower than $\sigma_{g,\mathrm{dB}} = 0.36$ dB of the 4C-MCF. The practical impact of the MDL is reported in [38] and [104], and for an acceptable capacity reduction of 10% at a 10^{-4} outage probability, a distance over 10 000 km can be achieved for the span configuration reported in [24].

A. Submarine Applications

Randomly-coupled MCFs are of particular interest for submarine systems because they can achieve a higher spatial density compared to SMFs or weakly-coupled MCFs. A recent trend in submarine systems, which are limited in electrical power supply, is to maximize the cable capacity by increasing the number of cores in the cable. This can be effectively achieved by replacing the SMFs utilized in current designs with randomly-coupled MCFs with the same cladding diameter. Therefore, the same cable design can be kept while increasing the number of cores up to 7

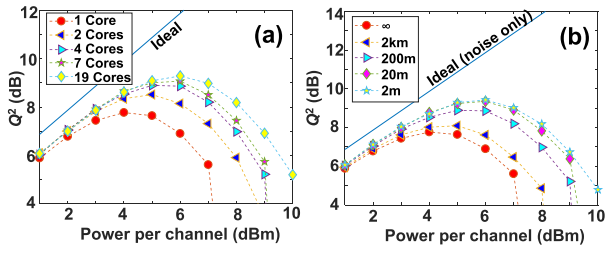

Fig. 22. *Q-factor versus power per channel and core for 15 channels for (a) various numbers of cores at a coupling length of 200 m and (b) various coupling lengths in the four-core fiber. (Replotted from the data in [99].)*

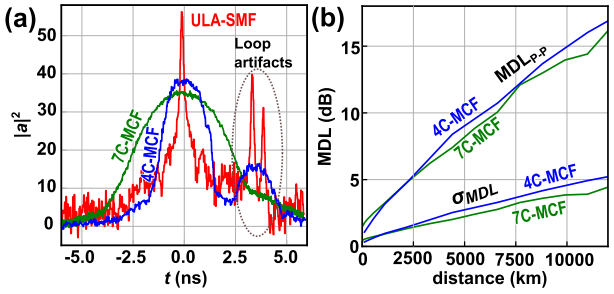

Fig. 23. *(a) Impulse response after 2200 km of ULA-SMF, 4C-MCF, and 7C-MCF. (b) MDL as a function of distance for 4C-MCF and 7C-MCF. (Replotted from the data in [24].)*

or more. As randomly-coupled MCFs can have transmission performance comparable to or better than SMFs, this represents a very compelling option for submarine cable. In order for randomly-coupled MCFs to be viable, it is, however, also important to demonstrate the availability of high-performance components, such as amplifiers supporting MCFs and low loss connectivity between fibers and components.

In addition, randomly-coupled MCFs require transceivers that support full MIMO processing between the cores. The added complexity of full MIMO transceivers was addressed in [105], and the results indicate that overall DSP complexity per core will only modestly increase (around 40% to support seven-core fibers), mostly because the DSP complexity in single-mode transceivers is dominated by the complexity of the chromatic dispersion compensation and the forward error correction. Practically, FPGA-based transceivers for four-core fibers have already been demonstrated over transoceanic distances [29], and more recently, a single FPGA-based transceiver supporting up to seven-core fibers has also been reported [96]. The translation into an ASIC-based solution—supporting higher symbol rates—is technologically feasible, and therefore, the MIMO complexity is currently not the limiting factor in the number of cores per fiber that can be supported in submarine applications.

B. Terrestrial Applications

Randomly-coupled MCFs could be used also in terrestrial systems, as they can significantly reduce the cross section of optical cables, which can have a significant impact on transportation and deployment costs. Furthermore, the improvement in nonlinear transmissions is more effective in terrestrial systems compared with power-limited submarine systems. Higher launching power thanks to the suppressed nonlinearity and relaxed electric power supply enables longer repeater spacing and, thus, may reduce the system cost.

In addition to optical amplifiers that support MCFs, new switching components supporting MCFs are required for multipoint terrestrial networks. For randomly-coupled cores, all the signals across the cores have to be routed together over the whole link length, and switches based on the joint switching architectures [106] are of particular interest. The switch that supports randomly-coupled MCFs would typically be composed of a waveguide shuffle that rearranges the core configuration at the entrance of the switch, followed by a wavelength selective switch in "joint switching" configuration, where a single steering element (microelectromechanical system (MEMS) or liquid crystal on silicon (LCOS) mirror) is used to switch all cores at the same time. At the output of the switch, a second core shuffle would be used to match the core arrangement of the randomly-coupled MCFs [107]. The disadvantage of this architecture is that randomly-coupled MCFs are not compatible with SMFs terrestrial networks, and there is no simple path to scale the number of cores over time.

Alternatively, randomly-coupled MCFs could be used as high-capacity dedicated links used in high-traffic links in parallel to traditional SMFs where needed.

VIII. CONCLUSION

Randomly-coupled MCF technologies have significantly advanced in the last decade. State-of-the-art randomly-coupled MCFs achieves simultaneously ultralow loss, large effective area, and higher core count, by breaking the tradeoff between the core density and optical properties in weakly-coupled MCFs. Random mode coupling requires MIMO DSP, but transmission experiments, including real-time trans-oceanic distance transmission, have proved that the sublinear accumulations of MD and MDL can reduce the complexity and outage probability of MIMO DSP. Nonlinear impairment suppression owing to random mode coupling has been confirmed in both theoretical studies and experiments. Low-loss connectivity technologies have been well developed, and conventional cabling technologies can realize favorable optical properties after deployment. These achievements already demonstrate the strong applicability of randomly-coupled MCFs to long-haul submarine transmission systems with limited cable cross sections. Although randomly-coupled MCFs can provide benefits even with SMF-based amplifiers, the realization of power-efficient multi-core amplifiers will further improve the transmission capacity of power-limited submarine systems. With further studies on switching technology and architectures, terrestrial networks can also be the application area of randomly-coupled MCFs. Since the power limitation of terrestrial systems can be relaxed compared to that of submarine systems, improvement in nonlinear transmissions will be more effective in terrestrial systems. ■

REFERENCES

[1] R. Essiambre and R. W. Tkach, "Capacity trends and limits of optical communication networks," *Proc. IEEE*, vol. 100, no. 5, pp. 1035–1055, May 2012.

[2] P. J. Winzer and D. T. Neilson, "From scaling disparities to integrated parallelism: A decathlon for a decade," *J. Lightw. Technol.*, vol. 35, no. 5, pp. 1099–1115, Mar. 1, 2017.

[3] P. J. Winzer, D. T. Neilson, and A. R. Chraplyvy, "Fiber-optic transmission and networking: The previous 20 and the next 20 years," *Opt. Exp.*, vol. 26, no. 18, pp. 24190–24239, Sep. 2018.

[4] A. Sano *et al.*, "102.3-Tb/s (224 × 548-Gb/s) C- and extended L-band all-Raman transmission over 240 km using PDM-64 QAM single carrier FDM with digital pilot tone," in *Proc. Opt. Fiber Commun. Conf.*, 2012, pp. 1–3, Paper PDP5C.3.

[5] F. Hamaoka *et al.*, "150.3-Tb/s ultra-wideband (S, C, and L bands) single-mode fibre transmission over 40-km using >519 Gb/s/λ PDM-128 QAM signals," in *Proc. Eur. Conf. Opt. Commun. (ECOC)*, Sep. 2018, pp. 1–3, Paper Mo4G.1.

[6] T. Morioka, "New generation optical infrastructure technologies: 'EXAT initiative' towards 2020 and beyond," in *Proc. OptoElectron. Commun. Conf. (OECC)*, Hong Kong, Jul. 2009, pp. 1–2, Paper FT4.

[7] K. Saitoh and S. Matsuo, "Multicore fiber technology," *J. Lightw. Technol.*, vol. 34, no. 1, pp. 55–66, Jan. 1, 2016.

[8] M.-J. Li and T. Hayashi, "Advances in low-loss, large-area, and multicore fibers," in *Optical Fiber Telecommunications VII*. New York, NY, USA: Academic, 2020, ch. 1, pp. 3–50.

[9] P. Sillard, "Few-mode fibers for space division multiplexing," in *Proc. Opt. Fiber Commun. Conf.*, Mar. 2016, pp. 1–53, Paper Th1J.1.

[10] P. J. Winzer, "Would scaling to extreme ultraviolet or soft X-ray communications resolve the capacity

crunch?" *J. Lightw. Technol.*, vol. 36, no. 24, pp. 5786–5793, Dec. 15, 2018.
[11] T. Hayashi, Y. Tamura, T. Hasegawa, and T. Taru, "Record-low spatial mode dispersion and ultra-low loss coupled multi-core fiber for ultra-long-haul transmission," *J. Lightw. Technol.*, vol. 35, no. 3, pp. 450–457, Feb. 1, 2017.
[12] H. Sakuma *et al.*, "Microbending behavior of randomly-coupled ultra-low-loss multi-core fiber," in *Proc. 45th Eur. Conf. Opt. Commun. (ECOC)*, 2019, pp. 1–3, Paper M.1.D.2.
[13] T. Sakamoto *et al.*, "Twisting-rate-controlled 125 μm cladding randomly coupled single-mode 12-core fiber," *J. Lightw. Technol.*, vol. 36, no. 2, pp. 325–330, Jan. 15, 2018.
[14] R. Ryf *et al.*, "Coherent 1200-km 6×6 MIMO mode-multiplexed transmission over 3-core microstructured fiber," in *Proc. Eur. Conf. Exhib. Opt. Commun. (ECOC)*, Geneva, Switzerland, pp. 1–3, Sep. 2011, Paper Th.13.C.1.
[15] K.-P. Ho and J. M. Kahn, "Statistics of group delays in multimode fiber with strong mode coupling," *J. Lightw. Technol.*, vol. 29, no. 21, pp. 3119–3128, Nov. 1, 2011.
[16] R. Ryf *et al.*, "Space-division multiplexed transmission over 4200-km 3-core microstructured fiber," in *Proc. Opt. Fiber Commun. Conf. (OFC)*, Mar. 2012, pp. 1–3, Paper PDP5C.2.
[17] C. Antonelli, A. Mecozzi, and M. Shtaif, "Delay spread in strongly coupled multi-core fibers for SDM transmission," in *Proc. Opt. Fiber Commun. Conf.*, Los Angeles, CA, USA, Mar. 2015, Paper Th4C.2.
[18] T. Sakamoto, T. Mori, M. Wada, T. Yamamoto, F. Yamamoto, and K. Nakajima, "Fiber twisting- and bending-induced adiabatic/nonadiabatic super-mode transition in coupled multicore fiber," *J. Lightw. Technol.*, vol. 34, no. 4, pp. 1228–1237, Feb. 15, 2016.
[19] T. Hayashi, "Multi-core fibers for space division multiplexing," in *Handbook of Optical Fibers*, G.-D. Peng, Ed. Singapore: Springer, Aug. 2019, pp. 99–145.
[20] C. Antonelli, A. Mecozzi, M. Shtaif, N. K. Fontaine, H. Chen, and R. Ryf, "Stokes-space analysis of modal dispersion of SDM fibers with mode-dependent loss: Theory and experiments," *J. Lightw. Technol.*, vol. 38, no. 7, pp. 1668–1677, Apr. 1, 2020.
[21] K.-P. Ho and J. M. Kahn, "Mode-dependent loss and gain: Statistics and effect on mode-division multiplexing," *Opt. Exp.*, vol. 19, no. 17, pp. 16612–16635, Aug. 2011.
[22] K.-P. Ho, "Exact model for mode-dependent gains and losses in multimode fiber," *J. Lightw. Technol.*, vol. 30, no. 23, pp. 3603–3609, Dec. 1, 2012.
[23] K.-P. Ho and J. M. Kahn, "Mode coupling and its impact on spatially multiplexed systems," in *Optical Fiber Telecommunications*, 6th ed., I. P. Kaminow, T. Li, and A. E. Willner, Eds. Amsterdam, The Netherlands: Elsevier, 2013, pp. 491–568.
[24] R. Ryf *et al.*, "Coupled-core transmission over 7-core fiber," in *Proc. Opt. Fiber Commun. Conf. (OFC)*, Mar. 2019, pp. 1–3, Paper Th4B.3.
[25] M. Arikawa, K. Nakamura, K. Hosokawa, and K. Hayashi, "Long-haul WDM/SDM transmission over coupled 4-core fiber with coupled 4-core EDFA and its mode dependent loss characteristics estimation," *J. Lightw. Technol.*, vol. 40, no. 6, pp. 1664–1671, Mar. 15, 2022.
[26] G. P. Agrawal and R.-J. Essiambre, "Nonlinear limits of SDM transmission," in *Proc. IEEE Photon. Soc. Summer Topical Meeting Ser.*, Jul. 2014, pp. 174–175.
[27] C. Antonelli, O. Golani, M. Shtaif, and A. Mecozzi, "Nonlinear interference noise in space-division multiplexed transmission through optical fibers," *Opt. Exp.*, vol. 25, no. 12, pp. 13055–13078, Jun. 2017.
[28] D. Soma, S. Beppu, H. Takahashi, N. Yoshikane, I. Morita, and T. Tsuritani, "Performance comparison for standard cladding ultra-low-loss uncoupled and coupled 4-core fibre transmission over 15,000 km," in *Proc. Eur. Conf. Opt. Commun. (ECOC)*, Dec. 2020, pp. 1–4, Paper Mo2E-4.
[29] S. Beppu *et al.*, "Real-time transoceanic coupled 4-core fiber transmission," in *Proc. Opt. Fiber Commun. Conf. (OFC)*, 2021, pp. 1–3, Paper F3B.4.
[30] D. Soma *et al.*, "50.47-Tbit/s standard cladding coupled 4-core fiber transmission over 9,150 km," *J. Lightw. Technol.*, vol. 39, no. 22, pp. 7099–7105, Nov. 15, 2021.
[31] G. Rademacher *et al.*, "High capacity transmission in a coupled-core three-core multi-core fiber," *J. Lightw. Technol.*, vol. 39, no. 3, pp. 757–762, Feb. 1, 2021.
[32] Y. Kokubun and M. Koshiba, "Novel multi-core fibers for mode division multiplexing: Proposal and design principle," *IEICE Electron. Exp.*, vol. 6, no. 8, pp. 522–528, 2009.
[33] C. Xia, N. Bai, I. Ozdur, X. Zhou, and G. Li, "Supermodes for optical transmission," *Opt. Exp.*, vol. 19, no. 17, pp. 16653–16664, Aug. 2011.
[34] C. Xia *et al.*, "Supermodes in coupled multi-core waveguide structures," *IEEE J. Sel. Top. Quantum Electron.*, vol. 22, no. 2, Mar./Apr. 2016, Art. no. 4401212.
[35] R. Ryf, R.-J. Essiambre, S. Randel, M. A. Mestre, C. Schmidt, and P. J. Winzer, "Impulse response analysis of coupled-core 3-core fibers," in *Proc. Eur. Conf. Opt. Commun. (ECOC)*, 2012, pp. 1–3, Paper Mo.1.F.4.
[36] T. Sakamoto *et al.*, "Experimental and numerical evaluation of inter-core differential mode delay characteristic of weakly-coupled multi-core fiber," *Opt. Exp.*, vol. 22, no. 8, pp. 31966–31976, 2014.
[37] B. Huang *et al.*, "Minimizing the modal delay spread in coupled-core two-core fiber," in *Proc. Conf. Lasers Electro-Opt.*, San Jose, CA, USA, Jun. 2016, pp. 1–2, Paper STu1F.3.
[38] P. J. Winzer and G. J. Foschini, "MIMO capacities and outage probabilities in spatially multiplexed optical transport systems," *Opt. Exp.*, vol. 19, no. 17, pp. 16680–16696, Aug. 2011.
[39] C. Antonelli, A. Mecozzi, M. Shtaif, and P. J. Winzer, "Modeling and performance metrics of MIMO-SDM systems with different amplification schemes in the presence of mode-dependent loss," *Opt. Exp.*, vol. 23, no. 3, pp. 2203–2219, Feb. 2015.
[40] A. Mecozzi, C. Antonelli, and M. Shtaif, "Intensity impulse response of SDM links," *Opt. Exp.*, vol. 23, no. 5, pp. 5738–5743, Mar. 2015.
[41] T. Fujisawa and K. Saitoh, "Group delay spread analysis of strongly coupled 3-core fibers: An effect of bending and twisting," *Opt. Exp.*, vol. 24, no. 9, pp. 9583–9591, Apr. 2016.
[42] T. Hayashi *et al.*, "Effects of core count/layout and twisting condition on spatial mode dispersion in coupled multi-core fibers," in *Proc. Eur. Conf. Opt. Commun. (ECOC)*, Düsseldorf, Germany, Sep. 2016, pp. 559–561, Paper W.2.B.5.
[43] R. Ryf *et al.*, "MIMO-based crosstalk suppression in spatially multiplexed 3×56-Gb/s PDM-QPSK signals for strongly coupled three-core fiber," *IEEE Photon. Technol. Lett.*, vol. 23, no. 20, pp. 1469–1471, Oct. 15, 2011.
[44] S. Randel *et al.*, "MIMO-based signal processing of spatially multiplexed 112-Gb/s PDM-QPSK signals using strongly-coupled 3-core fiber," in *Proc. 37th Eur. Conf. Opt. Commun. (ECOC)*, 2011, pp. 1–3, Paper Tu.5.B.1.
[45] T. Hayashi *et al.*, "Coupled-core multi-core fibers: High-spatial-density optical transmission fibers with low differential modal properties," in *Proc. Eur. Conf. Opt. Commun. (ECOC)*, Valencia, Spain, Sep. 2015, pp. 1–3, Paper We.1.4.1.
[46] T. Sakamoto, T. Mori, M. Wada, T. Yamamoto, and F. Yamamoto, "Fibre twisting and bending induced mode conversion characteristics in coupled multi-core fibre," in *Proc. Eur. Conf. Opt. Commun. (ECOC)*, Valencia, Spain, Sep. 2015, pp. 1–3, Paper P.1.2.
[47] R. Ryf *et al.*, "Space-division multiplexed transmission over 3×3 coupled-core multicore fiber," in *Proc. Opt. Fiber Commun. Conf.*, San Francisco, CA, USA, Mar. 2014, pp. 1–3, Paper Tu2J.4.
[48] R. Ryf *et al.*, "1705-km transmission over coupled-core fibre supporting 6 spatial modes," in *Proc. Eur. Conf. Opt. Commun. (ECOC)*, Cannes, France, Sep. 2014, pp. 1–3, Paper PD.3.2.
[49] E. S. Chou, T. Hayashi, T. Nagashima, J. M. Kahn, and T. Nakanishi, "Stable measurement of effective area in coupled multi-core fiber," in *Proc. Opt. Fiber Commun. Conf. (OFC)*, San Diego, CA, USA, Mar. 2018, pp. 1–3, Paper Th3D.4.
[50] M. Hirano *et al.*, "Record low loss, record high FOM optical fiber with manufacturable process," in *Proc. Opt. Fiber Commun. Conf.*, Mar. 2013, pp. 1–3, Paper PDP5A.7.
[51] T. Nakanishi, T. Hayashi, O. Shimakawa, and T. Sasaki, "Spatial-spectral-efficiency-enhanced multi-core fiber," in *Proc. Opt. Fiber Commun. Conf.*, Los Angeles, CA, USA, Mar. 2015, pp. 1–3, Paper Th3C.3.
[52] *Definitions and Test Methods for Linear, Deterministic Attributes of Single-Mode Fibre and Cable*, document ITU-T G.650.1, International Telecommunication Union, Mar. 2018.
[53] *Optical Fibres—Part 1–42: Measurement Methods and Test Procedures—Chromatic Dispersion*, International Standard IEC 60793-1-42:2013, International Electrotechnical Commission, 2013.
[54] N. K. Fontaine *et al.*, "Characterization of space-division multiplexing systems using a swept-wavelength interferometer," in *Proc. Opt. Fiber Commun. Conf. (OFC)*, Anaheim, CA, USA, 2013, pp. 1–3.
[55] M. Mazur *et al.*, "Transfer matrix characterization of field-deployed MCFs," in *Proc. Eur. Conf. Opt. Commun. (ECOC)*, Brussels, Belgium, Dec. 2020, pp. 1–4, Paper Th1A-3.
[56] G. D. VanWiggeren and D. M. Baney, "Swept-wavelength interferometric analysis of multiport components," *IEEE Photon. Technol. Lett.*, vol. 15, no. 9, pp. 1267–1269, Sep. 2003.
[57] J. P. Gordon and H. Kogelnik, "PMD fundamentals: Polarization mode dispersion in optical fibers," *Proc. Nat. Acad. Sci. USA*, vol. 97, no. 9, pp. 4541–4550, Apr. 2000.
[58] S. Fan and J. M. Kahn, "Principal modes in multimode waveguides," *Opt. Lett.*, vol. 30, no. 2, pp. 135–137, Jan. 2005.
[59] B. L. Heffner, "Automated measurement of polarization mode dispersion using Jones matrix eigenanalysis," *IEEE Photon. Technol. Lett.*, vol. 4, no. 9, pp. 1066–1069, Sep. 1992.
[60] N. Gisin, R. Passy, and J. P. von der Weid, "Definitions and measurements of polarization mode dispersion: Interferometric versus fixed analyzer methods," *IEEE Photon. Technol. Lett.*, vol. 6, no. 6, pp. 730–732, Jun. 1994.
[61] *Definitions and Test Methods for Statistical and Non-Linear Related Attributes of Single-Mode Fibre and Cable*, document ITU-T G.650.2, International Telecommunication Union, Aug. 2015.
[62] K. Choutagunta, S. O. Arik, K. P. Ho, and J. M. Kahn, "Characterizing mode-dependent loss and gain in multimode components," *J. Lightw. Technol.*, vol. 36, no. 18, pp. 3815–3823, Sep. 15, 2018.
[63] T. Hasegawa and T. Hayashi, "Measurement of mode dependent loss of randomly-coupled multi-core fiber using scrambling method," in *Proc. Optoelectron. Commun. Conf.*, Jul. 2021, pp. 1–3, Paper T2C.2.
[64] C. Antonelli, A. Mecozzi, M. Shtaif, and P. J. Winzer, "Nonlinear propagation equations in fibers with multiple modes—Transitions between representation bases," *APL Photon.*, vol. 4, no. 2, Jan. 2019, Art. no. 022806.
[65] E. Chou, T. Hayashi, T. Nagashima, J. M. Kahn, and T. Nakanishi, "Stable measurement of near/far field profiles of coupled multi-core fiber," in *Proc. 24th OptoElectron. Commun. Conf. (OECC) Int. Conf. Photon. Switching Comput. (PSC)*. Fukuoka, Japan: IEEE, Jul. 2019, pp. 1–3, Paper ThG3-1.
[66] M. Suzuki, H. Yoshii, T. Ito, Y. Yamamoto, T. Hayashi, and T. Hasegawa, "Low loss splicing between coupled multi-core fibers with thermally

expanded cores," in *Proc. Opt. Fiber Commun. Conf. (OFC)*, Mar. 2018, pp. 1–3, Paper Tu3B.5.
[67] T. Sakamoto *et al.*, "Characteristic of splicing misalignment induced mode dependent loss for coupled multi-core fibre," in *Proc. Eur. Conf. Opt. Commun. (ECOC)*, Sep. 2017, pp. 1–3, Paper W.3.B.4.
[68] T. Matsui, K. Nakajima, and P. Pondillo, "Weakly coupled multi-core fiber technology, deployments, and systems," *Proc. IEEE*, to be published.
[69] R. R. Thomson *et al.*, "Ultrafast-laser inscription of a three dimensional fan-out device for multicore fiber coupling applications," *Opt. Exp.*, vol. 15, no. 18, pp. 11691–11697, Sep. 2007.
[70] V. I. Kopp, J. Park, M. Wlodawski, J. Singer, D. Neugroschl, and A. Z. Genack, "Pitch reducing optical fiber array and multicore fiber for space-division multiplexing," in *Proc. IEEE Photon. Soc. Summer Topical Meeting*, Waikoloa, HI, USA, Jul. 2013, pp. 99–100, Paper TuC2.2.
[71] R. Ryf *et al.*, "Long-distance transmission over coupled-core multicore fiber," in *Proc. Eur. Conf. Opt. Commun. (ECOC)*, Düsseldorf, Germany, Sep. 2016, pp. 1–3, Paper Th.3.C.3.
[72] Y. Tottori, H. Tsuboya, T. Kobayashi, and M. Watanabe, "Integrated optical connection module for 7-core multi-core fiber and 7 single mode fibers," in *Proc. IEEE Photon. Soc. Summer Topical Meeting*, Jul. 2013, pp. 82–83.
[73] Y. Tottori, H. Tsuboya, and T. Kobayashi, "Improved return loss of fan-in/fan-out device for circular core array multi-core fiber using free space optics," in *Proc. IEEE Photon. Soc. Summer Topical Meeting Ser.*, Jul. 2014, pp. 166–167.
[74] Y. Jung, A. Wood, S. Jain, Y. Sasaki, S.-U. Alam, and D. J. Richardson, "Fully integrated optical isolators for space division multiplexed (SDM) transmission," *APL Photon.*, vol. 4, no. 2, Feb. 2019, Art. no. 022801.
[75] T. Takahata, Y. Minagawa, and T. Kobayashi, "Compact tap-isolator module using multicore fibre with practically low loss and small loss-variation," in *Proc. 45th Eur. Conf. Opt. Commun. (ECOC)*, Sep. 2019, pp. 1–4, Paper W.2.C.3.
[76] T. Takahata, A. Kaya, S. Nagayama, and T. Kobayashi, "Compact monitor device for multicore fibre with practically low loss using multiple lenses," in *Proc. Eur. Conf. Opt. Commun. (ECOC)*, Dec. 2020, pp. 1–4, Paper Th1A-6.
[77] T. Takahata, A. Kaya, Y. Ozawa, Y. Minagawa, and T. Kobayashi, "High reliability fan-in/fan-out device with isolator for multi-core fibre based on free space optics," in *Proc. Eur. Conf. Opt. Commun. (ECOC)*, Sep. 2021, pp. 1–3, Paper We1A.5.
[78] K. Watanabe, M. Takahashi, R. Sugizaki, and Y. Arashitani, "Four-core fan-in/fan-out applicable for o to L-band operation," in *Proc. 26th Optoelectron. Commun. Conf.*, Jul. 2021, pp. 1–3, Paper T2C.4.
[79] Y. Yamada *et al.*, "Development of novel optical fiber ribbon assembled into extremely high-density optical fiber cable," in *Proc. 61st Int. Cable Connectivity Symp. (IWCS)*, Oct. 2012, pp. 26–32.
[80] Y. Yamada *et al.*, "Design of high-density cable parameters for controlling spatial-mode dispersion of randomly coupled multi-core fibers," *J. Lightw. Technol.*, vol. 39, no. 4, pp. 1179–1185, Feb. 15, 2021.
[81] T. Hayashi, T. Nagashima, T. Muramoto, F. Sato, and T. Nakanishi, "Spatial mode dispersion suppressed randomly-coupled multi-core fiber in straightened loose-tube cable," in *Proc. Opt. Fiber Commun. Conf. (OFC)*, Mar. 2019, pp. 1–3, Paper Th4A.2.
[82] T. Hayashi *et al.*, "Field-deployed multi-core fiber testbed," in *Proc. 24th OptoElectron. Commun. Conf. (OECC) Int. Conf. Photon. Switching Comput. (PSC)*, Jul. 2019, pp. 1–3, Paper PDP 3.
[83] C. Antonelli *et al.*, "The city of L'Aquila as a living lab: The INCIPICT project and the 5G trial," in *Proc. IEEE 5G World Forum (5GWF)*, Jul. 2018, pp. 410–415.
[84] R. Ryf *et al.*, "Transmission over randomly-coupled 4-core fiber in field-deployed multi-core fiber cable," in *Proc. Eur. Conf. Opt. Commun. (ECOC)*. Brussels, Belgium: IEEE, Dec. 2020, pp. 1–4, Paper Mo2E-1.
[85] M. Mazur *et al.*, "Comparison of transfer matrix stability between a 110 km 7-core coupled-core multi-core fiber and single-mode fiber," in *Proc. Opt. Fiber Commun. Conf. (OFC)*, 2022, pp. 1–3, Paper M1E.2.
[86] M. Mazur *et al.*, "Real-time MIMO transmission over field-deployed coupled-core multi-core fibers," in *Proc. Opt. Fiber Commun. Conf. (OFC)*, San Diego, CA, USA, 2022, pp. 1–3, Paper Th4B.8.
[87] K. S. Abedin, M. F. Yan, T. F. Taunay, B. Zhu, E. M. Monberg, and D. J. DiGiovanni, "State-of-the-art multicore fiber amplifiers for space division multiplexing," *Opt. Fiber Technol.*, vol. 35, pp. 64–71, Feb. 2017.
[88] H. Chen *et al.*, "Integrated cladding-pumped multicore few-mode erbium-doped fibre amplifier for space-division-multiplexed communications," *Nature Photon.*, vol. 10, no. 8, pp. 529–533, Aug. 2016.
[89] T. Sakamoto, M. Wada, S. Aozasa, R. Imada, T. Yamamoto, and K. Nakajima, "Characteristics of randomly coupled 12-core erbium-doped fiber amplifier," *J. Lightw. Technol.*, vol. 39, no. 4, pp. 1186–1193, Feb. 15, 2021.
[90] H. Chen *et al.*, "Demonstration of cladding-pumped six-core erbium-doped fiber amplifier," *J. Lightw. Technol.*, vol. 34, no. 8, pp. 1654–1660, Apr. 15, 2016.
[91] N. K. Fontaine *et al.*, "Multi-mode optical fiber amplifier supporting over 10 spatial modes," in *Proc. Opt. Fiber Commun. Conf. (OFC)*, 2016, pp. 1–3, Paper Th5A-4.
[92] H. Takeshita, M. Sato, Y. Inada, E. L. T. de Gabory, and Y. Nakamura, "Past, current and future technologies for optical submarine cables," in *Proc. IEEE/ACM Workshop Photon.-Opt. Technol. Oriented Netw., Inf. Comput. Syst. (PHOTONICS)*, Nov. 2019, pp. 36–42.
[93] N. K. Fontaine *et al.*, "Coupled-core optical amplifier," in *Proc. Opt. Fiber Commun. Conf. (OFC)*, 2017, pp. 1–3, Paper Th5D-3.
[94] T. Ohtsuka, M. Tanaka, H. Sakuma, T. Hasegawa, T. Hayashi, and H. Tazawa, "Coupled 7-core erbium doped fiber amplifier and its characterization," in *Proc. Opt. Fiber Commun. Conf. (OFC)*, 2019, pp. 1–3, Paper W2A-19.
[95] M. Mazur *et al.*, "Transfer matrix characterization and mode-dependent loss optimization of packaged 7-core coupled-core EDFA," in *Proc. Eur. Conf. Opt. Commun. (ECOC)*, Sep. 2021, pp. 1–4, Paper Tu3A.6.
[96] M. Mazur *et al.*, "Real-time transmission over 2×55 km all 7-core coupled-core multi-core fiber link," in *Proc. Opt. Fiber Commun. Conf. (OFC)*, Mar. 2022, pp. 1–3, Paper Th4A.1.
[97] S. Mumtaz, R.-J. Essiambre, and G. P. Agrawal, "Reduction of nonlinear impairments in coupled-core multicore optical fibers," in *Proc. IEEE Photon. Soc. Summer Topical Meeting*, Jul. 2012, pp. 175–176.
[98] S. Mumtaz, R.-J. Essiambre, and G. P. Agrawal, "Reduction of nonlinear penalties due to linear coupling in multicore optical fibers," *IEEE Photon. Technol. Lett.*, vol. 24, no. 18, pp. 1574–1576, Sep. 15, 2012.
[99] R.-J. Essiambre, R. Ryf, and G. Rademacher, "System benefits of coupled-core multicore fibers with different coupling lengths," in *Proc. CLEO, Sci. Innov.*, 2018, pp. 1–3, Paper SM3C-2.
[100] A. Mecozzi, C. Antonelli, and M. Shtaif, "Nonlinear propagation in multi-mode fibers in the strong coupling regime," *Opt. Exp.*, vol. 20, no. 11, pp. 11673–11678, 2012.
[101] S. Mumtaz, R.-J. Essiambre, and G. P. Agrawal, "Nonlinear propagation in multimode and multicore fibers: Generalization of the Manakov equations," *J. Lightw. Technol.*, vol. 31, no. 3, pp. 398–406, Feb. 1, 2013.
[102] K. Shibahara, T. Mizuno, H. Ono, K. Nakajima, and Y. Miyamoto, "Long-haul DMD-unmanaged 6-mode-multiplexed transmission employing cyclic mode-group permutation," in *Proc. Opt. Fiber Commun. Conf. (OFC)*, Mar. 2022, pp. 1–3, Paper Th4A.1.
[103] T. Mizuno *et al.*, "12-core $\times$3-mode dense space division multiplexed transmission over 40 km employing multi-carrier signals with parallel MIMO equalization," in *Proc. Opt. Fiber Commun. Conf. (OFC)*, 2014, pp. 1–3, Paper Th5B.2.
[104] R. Ryf and C. Antonelli, "Space-division multiplexing," in *Springer Handbook of Optical Networks*. Cham, Switzerland: Springer, 2020. [Online]. Available: https://doi.org/10.1007/978-3-030-16250-4_10
[105] S. Randel, P. J. Winzer, M. Montoliu, and R. Ryf, "Complexity analysis of adaptive frequency-domain equalization for MIMO-SDM transmission," in *Proc. 39th Eur. Conf. Exhib. Opt. Commun. (ECOC)*, 2013, pp. 1–3, Paper Th2C.4.
[106] L. E. Nelson *et al.*, "Spatial superchannel routing in a two-span ROADM system for space division multiplexing," *J. Lightw. Technol.*, vol. 32, no. 4, pp. 783–789, Feb. 15, 2014.
[107] D. M. Marom, R. Ryf, and D. T. Neilson, "Networking and routing in space-division multiplexed systems," in *Optical Fiber Telecommunications VII*, A. E. Willner, Ed. New York, NY, USA: Academic, 2020, ch. 16, pp. 719–750.

ABOUT THE AUTHORS

Tetsuya Hayashi (Senior Member, IEEE) received the B.E. and M.E. degrees in electronic engineering from The University of Tokyo, Japan, in 2004 and 2006, respectively, and the Ph.D. degree in engineering from Hokkaido University, Sapporo, Japan, in 2013.

Since 2006, he has been with the Optical Communications Laboratory, Sumitomo Electric Industries Ltd., Yokohama, Japan, where he has been engaged in research and development on optical fibers and fiber optic technologies, and is currently the Group Leader for optical fiber research and development for space-division multiplexing. He has authored or coauthored more than 100 publications in international journals and conference proceedings, and three book chapters.

Dr. Hayashi is also a Senior Member of Optica (formerly OSA) and the Institute of Electronics, Information and Communication Engineers (IEICE). He received various awards and prizes, including the Tingye Li Innovation Prize from OSA at the Optical Fiber Communication Conference (OFC) 2017. He has served on and chaired many conference subcommittees, including OFC and the OptoElectronics and Communications Conference (OECC). He is also an Associate Editor of JOURNAL OF LIGHTWAVE TECHNOLOGY.

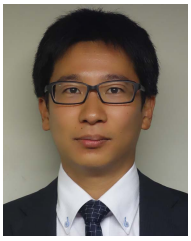

Taiji Sakamoto (Member, IEEE) received the B.E., M.E., and Ph.D. degrees in electrical engineering from Osaka Prefecture University, Osaka, Japan, in 2004, 2006, and 2012, respectively.

In 2006, he joined NTT Access Network Service Systems Laboratories, Ibaraki, Japan, where he has been engaged in research on optical fiber nonlinear effects, low nonlinear optical fiber, few-mode fiber, and multi-core fiber for optical multiple-input–multiple-output (MIMO) transmission systems. He is currently a Distinguished Researcher with NTT Access Network Service Systems Laboratories.

Dr. Sakamoto is also a member of Optica (formerly OSA) and the Institute of Electronics, Information and Communication Engineers (IEICE).

Yusuke Yamada received the B.E. and M.E. degrees in environmental system engineering from the Nagaoka University of Technology, Nagaoka, Japan, in 2003 and 2005, respectively.

In 2005, he joined NTT Access Network Service Systems Laboratories, Ibaraki, Japan, where he has been engaged in research on the optical fiber cable. He has been contributing to the activity of IEC SC86B in 2013–2014 and IEC SC86A since 2017. He is currently a Senior Research Engineer with NTT Access Network Service Systems Laboratories.

Mr. Yamada is also a member of the Institute of Electronics, Information, and Communication Engineers (IEICE) of Japan. He received the Best Paper Award at the 12th OptoElectronics and Communications Conference (OECC)/International Conference on Integrated Optics and Optical Fiber Communications (IOOC) in 2007.

Roland Ryf (Fellow, IEEE) received the Ph.D. degree in physics with a focus on nonlinear optics and optical parallel processing from the Swiss Federal Institute of Technology (ETH Zürich), Zürich, Switzerland, in 2000.

After joining Nokia Bell Labs, Murray Hill, NJ, USA, in 2000, he has been working on microelectromechanical system (MEMS)-based large port-count optical cross-connect switches, high-resolution optical wavelength filters, multimode components and optical amplifiers, and numerous first experimental demonstrations of long-distance high-capacity space-division multiplexed transmission over multimode fibers and coupled-core multicore fibers. He is currently a Bell Labs Fellow with Nokia Bell Labs. He has authored/coauthored over 400 journal and conference publications. He holds over 65 patents.

Dr. Ryf is also a Fellow of the Optical Society of America. He was a recipient of the 2018 William Streifer Award. He is actively involved with the IEEE Photonic Society and the Optical Society of America, serving as a Committee Member for various conferences, including the Conference on Lasers and Electro-Optics (CLEO) and the Optical Fiber Conference (OFC).

René-Jean Essiambre (Fellow, IEEE) received the Ph.D. degree in physics (optics) from Laval University, Quebec, QC, Canada, in 1994.

During his Ph.D. degree, he spent a year studying solid-state physics at McGill University, Montreal, QC, Canada. He pursued post-doctoral studies in optical communication at the Institute of Optics, University of Rochester, Rochester, NY, USA. In 1997, he joined Bell Labs, Holmdel, NJ, USA, part of Lucent Technologies (which became Alcatel-Lucent and is now Nokia), where he is currently a Distinguished Member of Technical Staff (DMTS) and a Bell Labs Fellow. He is also a Fellow of the Institute of Advanced Studies, Technical University of Munich (IAS-TUM), Munich, Germany, where he is also the Ambassador of the University. He worked on fiber lasers, nonlinear optics in fibers, coherent detection, advanced modulation formats, space-division multiplexing, information theory applied to optical fibers, and high-photon-efficiency systems. He has extensive knowledge and participated in the design of deployed commercial fiber-optic communication systems. He has given over 100 invited talks, and helped prepare and delivered the 2018 Physics Nobel Prize Lecture on behalf of Arthur Ashkin.

Dr. Essiambre was a member of the Board of Governors and is the President of the IEEE Photonics Society. He is also a Fellow of the Optica (formerly OSA). He was a recipient of the 2005 Engineering Excellence Award from OSA.

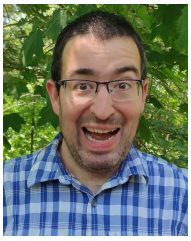

Nicolas Fontaine (Senior Member, IEEE) received the Ph.D. degree from the Next Generation Network Systems Laboratory in Electrical Engineering, University of California at Davis, Davis, CA, USA, in 2010. In his dissertation, he studied how to generate and measure the amplitude and phase of broadband optical waveforms in many narrowband spectral slices.

Since June 2011, he has been a member of Technical Staff at the Advanced Photonics Division, Bell Laboratories, Crawford Hill, NJ, USA. At Bell Laboratories, he develops devices for space-division multiplexing in multi-core and few-mode fibers, builds wavelength cross-connects and filtering devices, and investigates spectral slice coherent receivers for THz bandwidth waveform measurement.

Dr. Fontaine is also a Fellow of Optica.

Mikael Mazur (Member, IEEE) received the Ph.D. degree from the Chalmers University of Technology, Gothenburg, Sweden, in 2019. In his dissertation, he studied optical frequency combs in optical communications, focusing on signal processing schemes enabled by comb coherence.

In January 2020, he joined the Advanced Photonics Research Department, Nokia Bell Labs, Murray Hill, NJ, USA, as a member of Technical Staff. At Nokia Bell Labs, he develops subsystems and techniques for space-division multiplexing in coupled-core and multimode optical fibers, investigates multimode arbitrary waveform synthesis, and develops real-time signal processing techniques for optical transmission and fiber sensing systems.

Dr. Mazur is also a member of Optica.

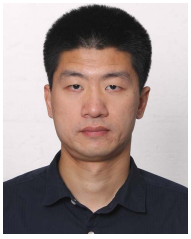

Haoshuo Chen (Senior Member, IEEE) received the Ph.D. degree *(cum laude)* in electrical engineering from the Eindhoven University of Technology (TU/E), Eindhoven, The Netherlands, in 2014.

Since December 2014, he has been a member of Technical Staff, Nokia Bell Labs, Murray Hill, NJ, USA. His main research interests include space-division multiplexing for telecommunication and imaging, dense photonic integration, power-efficient digital signal processing, fiber components, and wavelength/space switches.

Takemi Hasegawa (Member, IEEE) received the B.E. and M.E. degrees in electronic engineering from The University of Tokyo, Tokyo, Japan, in 1997 and 1999, respectively.

In 1999, he joined Sumitomo Electric Industries (SEI) Ltd., Yokohama, Japan. He has been engaged in research and development on optical fibers and photonic sensors. He is also a group manager engaged in the research and development of new optical fibers.

Mr. Hasegawa received the 2002 Hasunuma Prize from the Society of Instrument and Control Engineers.